Zymoseptoria tritici effectors structurally related to killer proteins UmV-KP4 and UmV-KP6 are toxic to fungi, and define extended protein families in fungi

Karine de Guillen[1], Léa Mammri[1], Jérôme Gracy[1], André Padilla[1], Philippe Barthe[1], François Hoh[1], Mounia Lahfa[1], Justine Rouffet[2], Yohann Petit-Houdenot[2], Thomas Kroj[3], Marc-Henri Lebrun[2,4]

[1] Centre de Biologie Structurale, Université de Montpellier, INSERM U1054, CNRS UMR 5048, 34090 Montpellier, France.

[2] Université Paris-Saclay, INRAE, UR BIOGER, Palaiseau, France

[3] PHIM Plant Health Institute, University of Montpellier, INRAE, CIRAD, Institut Agro, IRD, 34060 Montpellier, France.

[4] Université Paris-Saclay, CNRS, CEA, UMR I2BC, Gif sur Yvette, France

Corresponding Author:
Karine de Guillen
karine.deguillen@cbs.cnrs.fr
tel 33 467417708

Abstract 199 words

Fungal effectors play crucial roles in plant infection. Despite low sequence identity, effectors were recently classified into structural families. In this study, we have elucidated the structures of Zt-NIP1 and Mycgr3-91409 effectors of the wheat fungal pathogen *Zymoseptoria tritici,* using X-ray crystallography and NMR. These effectors displayed a structural homology with, respectively, KP4 and KP6α killer toxins, from UmV dsRNA viruses infecting the corn fungal pathogen *Ustilago maydis*. Consequently, Zt-NIP1 and Mycgr3-91409 were renamed Zt-KP4-1 and Zt-KP6-1. Orthologs and paralogs of Zt-KP4-1 and Zt-KP6-1 were identified in *Zymoseptoria*, but not in other fungi, except Ecp2 effectors related to Zt-KP4-1. Assessment of the biological activities of Zt-KP6-1 and Zt-KP4-1 revealed their toxicity to fungi such as *Botrytis cinerea* and *Z. tritici*, but not to wheat. A novel pipeline relying on Foldseek and cysteine-pattern constrained HMM searches of AlphaFold2 predicted structures from Uniprot generated a comprehensive inventory of KP4 and KP6 proteins in fungi and plants. A structure-based classification of these proteins revealed four KP4 and three KP6 structural super families. This classification provided far-reaching hypotheses on their biological function and evolution. This unifying structural framework highlights the power of structure determination for the classification of effectors, and their functional investigation.

INTRODUCTION

Fungal plant pathogens secrete large repertoires of effectors during host plant infection mostly composed of small proteins without enzymatic functions [1,2]. Most fungal effectors display no or very limited protein sequence similarities [3,4]. However, the comparison of their three-dimensional structures allows their classification into families of structurally related proteins [3]. This strategy was successful in identifying a large number of avirulence (AVR) and ToxB-like effectors from the fungal rice pathogen *Pyricularia oryzae* sharing the same conserved fold and called MAX effectors [5–7]. The RNase-like proteins associated with haustoria (RALPH) effectors of the cereal powdery mildew fungus *Blumeria graminis* were also grouped into a family of structurally related proteins using modeling and experimental structure determination [8–11]. Additional structural families of fungal effectors were identified using experimental structure determination and modeling in *Leptosphaeria maculans* [12–15], *Fusarium oxysporum* [16,17], and *Venturia inaequalis* [18]. Recently, the systematic prediction of structures of secreted fungal proteins with different programs including AlphaFold2 (AF2) [19], revealed novel structural families of fungal effectors [20,21].

To identify novel families of fungal effectors, we elucidated the three-dimensional structures of the secreted proteins Zt-Mycgr3-91409 and Zt-NIP1 from the wheat fungal pathogen *Zymoseptoria tritici* by X-ray diffraction (XRD) and nuclear magnetic resonance (NMR). Zt-Mycgr3-91409 is an effector upregulated during infection of wheat leaves [22] previously suggested to be a MAX effector [5]. Zt-NIP1 is expressed during infection of wheat [22,23] and induces mild chlorotic lesions on wheat leaves [24]. Unexpectedly, the structures of Zt-Mycgr3-91409 and Zt-NIP1 shared structural similarities with UmV-KP6α and UmV-KP4 killer proteins (KP) toxins encoded by dsRNA viruses infecting the corn fungal pathogen *Ustilago maydis*. UmV-KP6α and UmV-KP4 kill susceptible *U. maydis* strains, while UmV infected strains are resistant to the killer toxin they produce [25,26]. Consequently, we renamed Zt-Mycgr3-91409 to Zt-KP6-1 and Zt-NIP1 to Zt-KP4-1. Bioassays revealed that Zt-KP6-1 and Zt-KP4-1 were toxic to fungi, but not to wheat. Proteins structurally related to Zt-KP6-1 or Zt-KP4-1 were widely distributed across fungi, and classified into a unifying framework of structural families.

78 **RESULTS**

79

80 **Zt-Mycgr3-91409-2 is a structural homolog of UmV-KP6 killer toxin**

81

82 The *Zt-Mycgr3-91409* gene model was curated according to transcript evidence [27]
83 (Sup Figure 1A). The corresponding protein, Zt-Mycgr3-91409-2 (SMR48303,
84 A0A2H1G421) was expressed without its secretion signal in *Escherichia coli* and
85 purified by affinity and size exclusion chromatography (SEC) (Sup File S1, Sup Figure
86 2). High-resolution diffracting crystals were obtained after optimization of Li_2SO_4
87 concentration and pH and soaked in tantalum. Analyses of X-Rays Diffraction data
88 (XRD) at 1.36 Å resolution showed that crystals belonged to the $P2_12_12_1$ space group
89 with two copies of the protein per asymmetric unit. The structure of Zt-Mycgr3-91409-
90 2 was solved by single-wavelength anomalous diffraction (SAD), revealing a protein
91 with a typical α/β sandwich structure (Figure 1, Sup Table 1). This fold has two α-
92 helices and four β-strands arranged in an antiparallel β-sheet with one hairpin
93 connection formed by β2-β3 and two βαβ connections, which placed the α-helices in
94 an antiparallel manner on one side of the β-sheet.

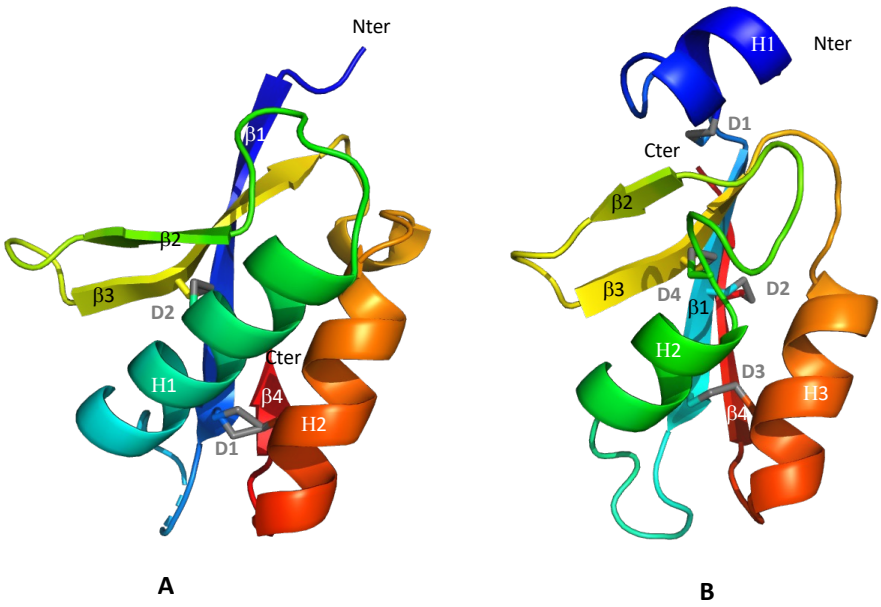

Figure 1

95

Figure 1. *Crystal structures of (A) Zt-KP6-1 (6QPK chain A) and (B) UmV-KP6α (4GVB chain A).*

(A) Zt-Mycgr3-91409-2 was renamed to Zt-KP6-1 according to its structural homology to UmV-KP6α (see text). Structures were coloured in rainbow colours from blue (N terminus) to red (C terminus). For Zt-KP6-1, the loop connecting β1 (in blue) to H1 (in cyan) was not observed in the density map and is shown as a blue dashed line. Disulphide bonds are shown in grey and labelled Dx. For the D1 (C26-C86) bond in Zt-KP6-1, both conformations are shown.

The α-helix H2 was preceded by a 3^{10} helix formed by residues 77 to 89 (numbering according to the mature protein). Both α-helices (H1 and H2) were tightly packed against the β-sheet, with one disulphide bond formed between cysteine residues in β1 (Cys26) and H2 (Cys86) and another disulphide bond formed between cysteine residues in H1 (Cys43) and β3 (Cys65), making the fold very compact. Alternative conformations were observed for Cys26 involving the disulphide bond with Cys86. The interface area between the two monomers observed in the crystal, determined by PDBePISA, was estimated to be 435.8Å^2. The Complexation Significance Score (CSS) was 0, indicating that the dimer has no biological relevance and resulted from crystal packing. NMR studies of the protein labelled with ^{15}N revealed a high similarity to the crystal structure, with an r.m.s.d. of 0.7 ± 0.6 Å on structured parts. However, the protein was not dimeric in solution, as shown by the narrowness of the ^{1}H-^{15}N HSQC spectrum peaks (Sup Figure 3 and Sup Table 2), and the single elution profile at 95 min observed in SEC corresponding to a retention time of a 9 kDa globular protein (Sup Figure 2).

A DALI analysis [28] revealed a structural similarity between Zt-Mycgr3-91409-2 and UmV-KP6α (PDB 4GVB, Figure 1, Z-score of 6.7 and r.m.s.d of 2.5 Å for 63 aligned residues). UmV-KP6α is produced together with UmV-KP6β by cleavage of the UmV-KP6 pre-protein encoded by a dsRNA virus infecting *U. maydis,* a fungal pathogen causing corn smut disease [26]. Both mature proteins have a highly similar fold [26,29] defined by two α-helices (H1 and H2) positioned on one side of a 4-stranded β-sheet, with a β4-β1-H1-β3-H2-β2 topology (KP6 fold), also observed for Zt-KP6-1 (Sup Figure 4). All three proteins have two right handed β-α-β split crossovers, which distinguish the KP6 fold from toxins of similar size [30]. Another characteristic of the KP6 fold was

130 the two disulphide bonds that linked the antiparallel α-helices to the central β-sheet of
131 the protein (Sup. Figure. 4). However, Zt-KP6-1 did not have the N-terminal
132 hydrophobic α-helix extension found in UmV-KP6α. According to these structural
133 similarities, Zt-Mycgr3-91409-2 was renamed Zt-KP6-1.
134
135 **Zt-NIP1 is a structural homolog of *UmV*-KP4 killer toxin**
136
137 Zt-NIP1 was identified as a wheat necrosis-inducing protein produced by IPO323 *Z.*
138 *tritici* isolate during wheat leaf infection [24]. However, the CDS at the *Zt-NIP1* locus in
139 IPO323 genome (*Zt-Mycgr3-106176*) encoded a protein with a sequence unrelated to
140 NIP1. We re-annotated the locus by predicting a new CDS in agreement with transcript
141 evidence and almost identical to NIP1 (99% identity) [27] (Sup Figure 1B). Zt-NIP1
142 (SMR6055, A0A2H1H404) was expressed in *E. coli* (Sup File S1) and purified by
143 affinity chromatography and SEC. SEC revealed an equilibrium between Zt-NIP1
144 monomers and dimers in solution (Sup Figure 5). High-resolution diffracting crystals
145 were obtained and belonged to the *H3* space group with 8 copies of the protein per
146 asymmetric unit (Sup Table 1). The Zt-NIP1 structure was solved by molecular
147 replacement using an AF2 model (Figure 2) revealing a typical α/β sandwich fold with
148 a single split βαβ motif and two disulphide bonds. A main antiparallel 5-stranded β-
149 sheet formed by β1-β3-β4-β6-β7, was packed against two α-helices (H1 and H2) and
150 combined with a second, small antiparallel two-stranded β-sheet comprising β2 and β5
151 (with 4 residues each). The fold was held together by two disulphide bonds formed
152 between cysteine residues in β2 (Cys39) and β7 (Cys142), and H1 (Cys60) and β4
153 (Cys89). Chains E-H, G-B, F-C, and D-A formed dimers, through the main 5-stranded
154 β-sheet with an average interface area of 852.2 $Å^2$ determined by PDBePISA. These
155 dimers exhibited a CSS score of 1.0, supporting the biological significance of dimer
156 formation (Sup Figure 6).
157

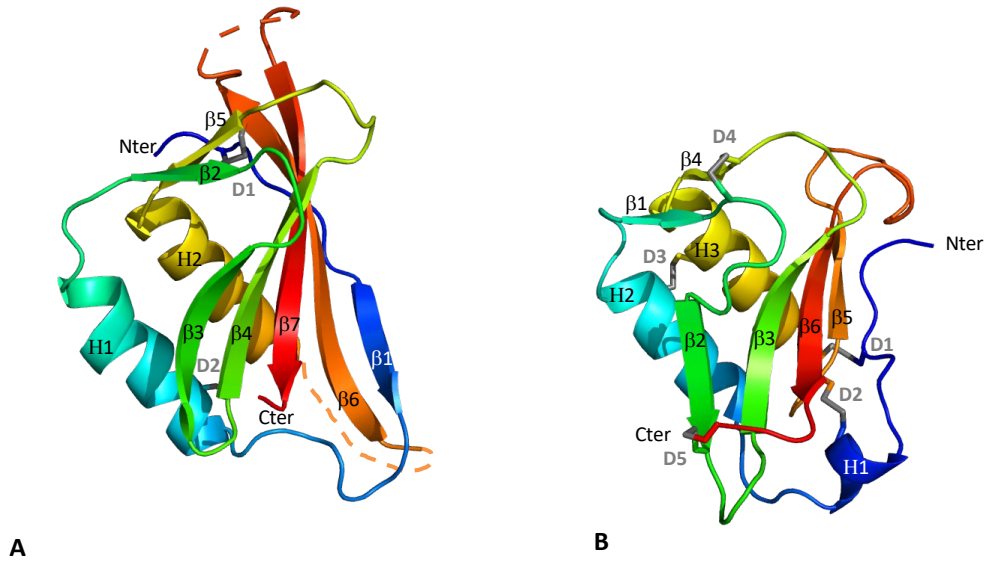

Figure 2

Figure 2. *Crystal structures of (A) Zt-KP4-1 (8ACX chain A) and (B) UmV-KP4 (1KPT chain A).*
(A) Zt-NIP1 was renamed to Zt-KP4-1 according to its structural similarity to UmV-KP4 using DALI (see main text). Structures were coloured in rainbow colours from blue (N terminus) to red (C terminus). For Zt-KP4-1 the loops connecting β6 to β7 and β6 to H1 were not observed in the density map and were shown as dashed lines. Disulphide bonds are shown in grey and labelled Dx.

A DALI analysis [28], revealed structural similarity between Zt-NIP1 and UmV-KP4 (PDB 1KPT, Figure 2). UmV-KP4, like UmV-KP6 is encoded by a dsRNA virus infecting *U. maydis* [26]. The two proteins superposed with a Z-score of 7.3 and a r.m.s.d value of 2.4 Å (82 residues aligned). UmV-KP4 [31,32] belongs to the α/β sandwich family of proteins and is composed of seven β strands and three α-helices. Similar to Zt-NIP1, UmV-KP4 has two helices (H2 and H3) in a left-handed βαβ crossover conformation, which is a rare structural feature (Sup Figure 7) [30]. The main difference between the two proteins is the presence of a β-strand (β1) at the N-terminus for Zt-NIP1 instead of a short α-helix (H1) for UmV-KP4. The two proteins also differ in the number and

177 location of disulphide bonds. While Zt-NIP1 has two disulphide bonds (as described
178 above), UmV-KP4 has five. Based on the structural similarity of these proteins, Zt-NIP1
179 was renamed to Zt-KP4-1.
180
181 **Zt-KP4 and Zt-KP6 are toxic to fungi**
182
183 When Zt-KP4-1 or Zt-KP6-1 (2 μM) were infiltrated into leaves of the wheat cultivar
184 Taichung 29, which is susceptible to *Z. tritici*, they did not induce visible signs of toxicity
185 such as leaf chlorosis or necrosis. The necrotrophic effector ToxA from *P. nodorum*
186 [33], used as a positive control in this experiment, induced typical necrotic lesions. To
187 test if Zt-KP4-1 and Zt-KP6-1 were toxic to fungi, we monitored their effect on the
188 growth of the model fungal plant pathogen *Botrytis cinerea* and of *Z. tritici* isolate
189 IPO323, which carries both Zt-KP4-1 and Zt-KP6-1. The protein concentrations used
190 in these experiments were within the range of 0.5 to 5.5 μM. These concentrations
191 were below those commonly used for the investigation of fungal toxic proteins which
192 are generally in the range of 20 μM [34,35]. Zt-KP4-1 strongly inhibited the growth of
193 both fungi at 5.5 μM (91-95 % inhibition, Table 1). At 1.65 μM, it only inhibited *Z. tritici*
194 (48 % inhibition, Table 1). Zt-KP6-1 strongly inhibited the growth of *B. cinerea* (94 %
195 inhibition at 5.5 μM, Table 1), but had only a weaker effect on *Z. tritici* growth (24 %
196 inhibition at 5.5 μM, Table 1). These results showed that Zt-KP4-1 and Zt-KP6-1 are
197 toxic to fungi, but not to wheat. While Zt-KP4-1 displayed the same toxicity on *Z. tritici*
198 and *B. cinerea,* Zt-KP6-1 showed selectivity, as it was four times more active on *B.*
199 *cinerea* than on *Z. tritici*.
200
201

		% inhibition	
		Botrytis cinerea	***Zymoseptoria tritici***
Protein concentration (µM)			
TOX A	5.50	25 ± 1.4	0
	1.65	0	0
	0.55	0	0
Zt-KP4-1	5.50	91 ± 3.2	95 ± 1.4
	1.65	0	48 ± 2.2
	0.55	0	25 ± 1.4
Zt-KP6-1	5.50	94 ± 2.0	24 ± 1.2
	1.65	0	0
	0.55	0	0

Table 1. *Toxicity of Zt-KP4-1 and Zt-KP6-1 to fungi*

The percentages of B. cinerea *and* Z. tritici *growth inhibition were calculated for different concentrations of ToxA, Zt-KP4-1and Zt-KP6-1. Values are the mean ± Standard Error of the Mean (SEM) from three experiments.*

Identification of Zt-KP6-1 homologs in *Zymoseptoria*

Proteins with sequences highly similar to Zt-KP6-1 were identified in other strains of *Z. tritici* [36] and *Z. pseudotritici* (Zp-KP6-1, 92% identity, Figure 3), but not in other fungi, including available genomes from other *Zymoseptoria* species. Proteins with a low sequence identity to Zt-KP6-1 (28-30%) were identified in *Z. tritici* (Zt-KP6-2) and other *Zymoseptoria* species (KP6-2 from *Z. brevis, Z. arbibiliaie* and *Z. pseudotritici*, Figure 3) but not in other fungi. The structure of the Zt-KP6-2 protein predicted by AF2 was highly similar to that of Zt-KP6-1 (Z-score of 12.1; r.m.s.d of 1.9 Å for 73 aligned residues, Sup Figure 8). However, it contained an 11 amino acid C-terminal sequence with two cysteine residues conserved in all KP6-2 proteins, but absent from KP6-1 proteins. The phylogenetic analysis of KP6-1 and KP6-2 proteins highlighted two clades gathering orthologous proteins from different *Zymoseptoria* species and suggesting that *Zymoseptoria* KP6-1 and KP6-2 are paralogs originating from the duplication of an ancestral gene before the divergence of the respective species (Figure 3).

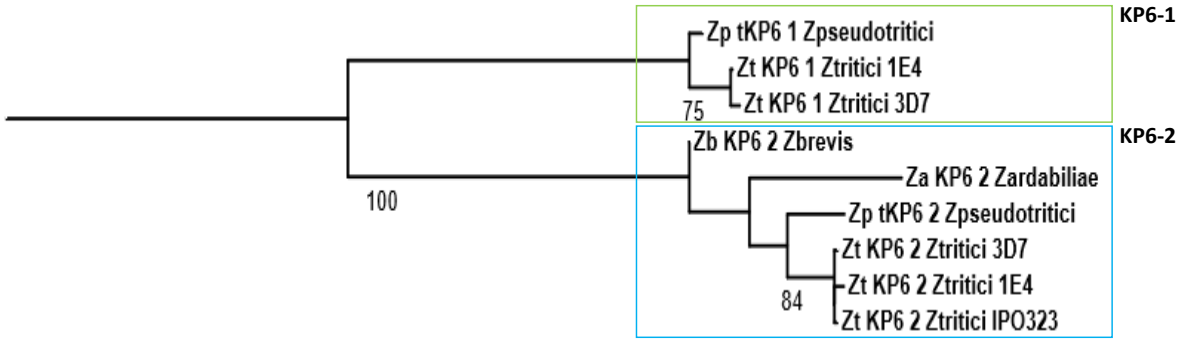

Figure 3. Phylogenetic tree of *Zymoseptoria* KP6-1 and KP6-2

MAFFT alignment, BMGE cleaning, PhyML Phylogenetic tree using NGPhylogeny.fr. [37] Bootstrap values > 70% are indicated under each branch after the supported node. Midpoint tree rooting. Zt-KP6-1_Ztritici_3D7: Uniprot A0A1X7RM13 (identical to Zt-KP6-1_IPO323); Zt-KP6-1_Ztritici_1E4: Uniprot A0A2H1G421, PDB 6QKP; Zp-KP6-1_Zpseudotritici: JGI Zymps1_802032; Zt-KP6-2_Ztritici_1E4: Uniprot A0A2H1H0K4; Zt-KP6-2_Ztritici_IPO323: Uniprot F9XLY9; Zt-KP6-2_Ztritici_3D7: Uniprot A0A1X7S5L2; Zb-KP6-2_Zbrevis: Uniprot A0A0F4GMG5; Za-KP6-2_Zardabiliae: JGI Za_774343 ; Zp-KP6-2_Zpseudotritici: JGI Zymps1_805921.

Using a novel pipeline based on FoldSeek and Hmmer (FHAT, Foldseek Hmmer Alphafold TMalign, Sup Figure 9), we identified four additional candidate KP6 proteins in *Zymoseptoria.* Visual inspection of their AF2-predicted structures revealed important overlap with the Zt-KP6-1 structure for three of them: Zt-KP6-4, Zt-KP6-5 and Zb-KP6-6. The remaining one, Zt-KP6-3, displayed a low structural similarity with KP6-1 (DALI score of 0) and it was excluded from further analyses. Overall, *Zymoseptoria* had five different KP6 proteins with low or no sequence similarity, but sharing a similar three-dimensional structure.

Identification of Zt-KP4-1 homologs in *Zymoseptoria*

Proteins with sequences highly similar to Zt-KP4-1 were identified in other strains of *Z. tritici* [36] (Figure 4), but not in other *Zymoseptoria* species. Proteins with a low sequence identity to Zt-KP4-1 (33-35%) were identified in *Z. tritici* (Zt-KP4-2; Zt-KP4-3) and *Z. brevis* (Zb-KP4-2; Zb-KP4-3). The AF2 structures of the Zt-KP4-2 and Zt-KP4-3 proteins predicted by AF2 were highly similar to that of Zt-KP4-1 (Zt-KP4-2: Z-

score of 16.5; r.m.s.d of 1.6 Å for 111 aligned residues, Zt-KP4-3: Z-score of 15.8; r.m.s.d of 1.7 Å for 110 aligned residues Sup Figure 10). BlastP searches of the proteomes of other fungi with Zt-KP4-1 or Zt-KP4-2 as queries, retrieved proteins related to the effector ECP2 (ExtraCellular Protein 2) from the tomato pathogen *Passalora fulva* (syn. *Cladosporium fulvum*) [38,39] Yet, the similarity scores were low (28-32% identity, e-value 10^{-20}). A phylogenetic analysis of *Zymoseptoria* KP4-1, KP4-2 and KP4-3 proteins including ECP2 proteins as outgroups [38].The *Zymoseptoria* KP4-1, KP4-2 and KP4-3 proteins clustered as three independent clades gathering orthologous proteins from *Zymoseptoria* rooted by the ECP2 proteins (Figure 4). This topology suggested that KP4-1, KP4-2 and KP4-3 originated from duplications of an ancestral ECP2-related gene, prior to the divergence of *Zymoseptoria* species.

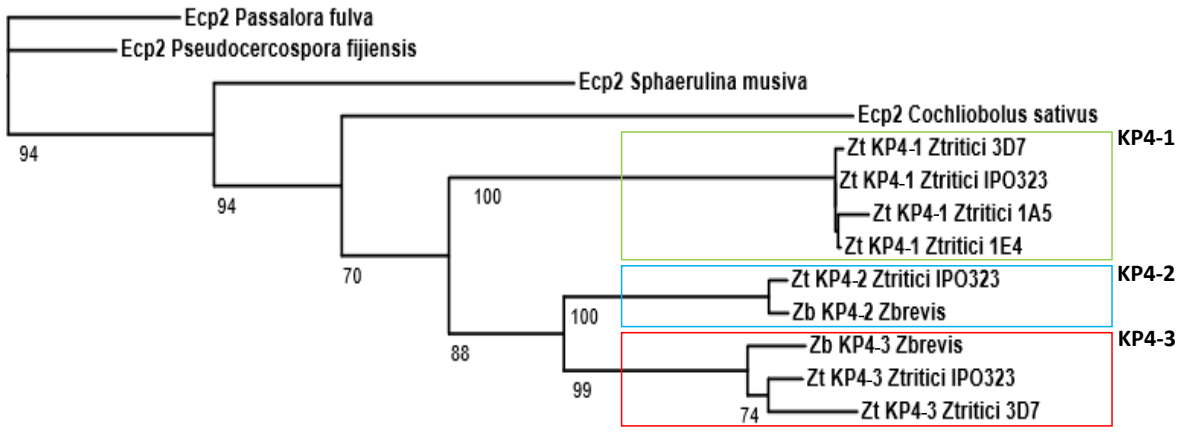

Figure 4: Phylogenetic tree of *Zymoseptoria* KP4-1, KP4-2 and KP4-3

MAFFT alignment, BMGE cleaning, PhyML Phylogenetic tree using NGPhylogeny.fr [37]. Bootstrap values > 70% are indicated under each branch after the supported node. Tree root with Ecp2_Passalora fulva and Ecp2_Pseudocercospora fijiensis as outgroups. Zt-KP4-1_Ztritici_IPO323: re-annotated NIP1/Mycgr3-106176 see Sup. Fig1; Zt-KP4-1_Ztritici_1E4: Uniprot A0A2H1H404; Zt-KP4-1_Ztritici_3D7: Uniprot A0A1X7S6U3; Zt-KP4-1_Ztritici_1A5: Uniprot A0A1Y6M012; Zt-KP4-2_Ztritici_IPO323: Mycgr3-107904, Uniprot F9X223; Zb-KP4-2_Zbrevis: KJY02238, Uniprot A0A0F4GYX0; Zt-KP4-3_Ztritici_IPO323: Mycgr3-111636, Uniprot F9XQ02; Zt-KP4-3_Ztritici_3D7: Uniprot A0A1X7S9R6; Zb-KP4-3_Zbrevis: KJX96086, Uniprot A0A0F4GF74; Ecp2_Passalora fulva: Uniprot Q00365; Ecp2_Pseudocercospora

277 *fijiensis: Uniprot M2Z6V3; Ecp2_Sphaerulina musiva: Uniprot N1QK49;*
278 *Ecp2_Cochliobolus sativus: Uniprot M2TE34*
279
280 A previous large-scale comparative genomics study of fungal effectors outlined the
281 HCE2 superfamily widely distributed in fungi (HCE2: Homologs of *C. fulvum* Ecp2)[39].
282 This analysis established a novel pfam domain (HCE2, PF14856) to identify proteins
283 related to Ecp2. We detected the HCE2 domain in Zt-KP4-1, Zt-KP4-2 and Zt-KP4-3,
284 which is consistent with their sequence similarity to *C. fulvum* Ecp2. However, we did
285 not detect additional *Z. tritici* proteins with a HCE2 domain. Using FHAT (Sup Figure
286 9), we identified six additional candidate KP4 proteins in *Zymoseptoria*. Visual
287 inspection of their AF2-predicted structures revealed important overlap with the Zt-
288 KP4-1 structure for four of them: Zt-KP4-5, Zt-KP4-6, Zt-KP4-7 and Zt-KP4-9. The
289 remaining ones, Zt-KP4-4 and Zt-KP4-8, displayed only a low structural similarity to Zt-
290 KP4-1 despite the presence of the same number of α–helices and β strands and a
291 similar organization. In Zt-KP4-4, the structures of the β2 and β5 strands were not well
292 defined (twisted), and the β2-β3 and β5-β6 interactions were reduced. In Zt-KP4-8, the
293 interactions between the β1 and β4 strands were missing. These two proteins were
294 therefore excluded from further analyses. Overall, *Zymoseptoria* has seven KP4
295 proteins with low or no sequence similarity, but sharing the same three-dimensional
296 structure.
297
298 ***Zymoseptoria KP4* and *KP6* are expressed during infection**
299
300 Published IPO323 RNA-Seq data [22] showed that *Zt-KP4-1* was the most highly
301 expressed *Zt-KP4* gene during infection of wheat leaves (25 x beta-tubulin *TUB1*), with
302 maximum expression at 9 dpi (Sup Fig. 11). It was also expressed during *in vitro*
303 growth, although to a lesser extent. *Zt-KP4-3* was highly expressed during infection at
304 9 and 14 dpi (10 x *TUB1*), and during *in vitro* growth. *Zt-KP4-2* was constitutively
305 expressed at a level similar to *TUB1*. *Zt-KP4-5, Zt-KP4-6* and *Zt-KP4-7* were
306 expressed at low levels (1/10th of *TUB1*) in all analysed conditions, while *Zt-KP4-9* was
307 not expressed. *Zt-KP6-1*, *Zt-KP6-2*, *Zt-KP6-4* and *Zt-KP6-6* displayed a similar
308 expression pattern with maximum expression during infection at 9 dpi (1 to 2 x *TUB1*),
309 and highly reduced expression during *in vitro* growth (100 fold less than during
310 infection). *Zt-KP6-5* was not expressed. In summary, this survey showed that most

311 *Zymoseptoria KP4* and *KP6* were over-expressed during infection at the switch from
312 the asymptomatic phase to the necrotrophic phase (9-14 dpi). This switch is associated
313 with the massive colonization of the apoplast of the infected wheat leaf by infectious
314 hyphae of *Z. tritici*, and the invasion of sub-stomatal cavities where they differentiate
315 into pycnidia [40].
316
317 **Proteins with a KP6 fold are widespread in fungi**
318
319 To establish a comprehensive inventory of proteins structurally related to Zt-KP6-1 in
320 fungi, we searched 1014 fungal genomes for structurally related proteins using a novel
321 Fold-Seek/Hmmer pipeline (Sup Figure 9). After filtering of results for significant
322 structural similarity to Zt-KP6-1 or UmV-KP6α using TM align (TM-score above 0.5)
323 [41], this analysis identified 2556 KP6 candidates belonging to 81 AFDB50 clusters
324 (kclXX-Y), which we merged into 17 meta-clusters (kclXX) (Sup Figure 9). Visual
325 inspection of the structures of one representative protein from each meta-cluster
326 rejected 10 meta-clusters with topologies different from the typical KP6 fold. The
327 remaining 7 KP6 FHAT meta-clusters gathered 1307 proteins (final KP6 FHAT
328 database) including, Zt-KP6-1 (kcl06), Zt-KP6-2 (kcl06), Zt-KP6-4 (kcl02), Zt-KP6-5
329 (kcl07), Zt-KP6 (kcl07) (sup Table 3). Several fungal effectors have been described as
330 structurally related to UmV-KP6α: ECP28 from *C. fulvum* [42], AvrLm10A and AvrLm6
331 from *L. maculans* [14,15], SIX5 from *Fusarium oxysporum* [14], BAS4 from *Pyricularia*
332 *oryzae* [43], and Cb-Nip1 from *Cercospora beticola* [44]. In addition, the systematic
333 analysis of effector structures of *V. inaequalis* and *L. maculans* found 108 and 13
334 proteins structurally related to KP6, respectively [15,18]. Only few of these proteins
335 were identified in our analysis, since most sequences were not available in Uniprot. A
336 visual inspection of the structural overlaps between these additional KP6 proteins and
337 Zt-KP6-1 rejected only Cb-NIP1, since its AF2 model was not sufficiently structured to
338 allow its superposition to Zt-KP6-1. To search for structural relationships among KP6
339 proteins, we selected at least one representative of each of the 7 KP6 FHAT meta-
340 clusters, one representative of each KP6 family identified in *L. maculans* (8 families)
341 [15], one representative of each major KP6 family identified in *V. inaequalis* (4 families)
342 [18] as well as UmV-KP6α and UmV-KP6β. This selection of 35 KP6 included all
343 *Zymoseptoria* KP6 (Zt-KP6-1, 2, 4, 5, 6) and known KP6 (Six5, AvrLm10A, BAS4,
344 AvrLm6, ECP28). The similarity between the structures of these 35 proteins was

assessed using a principal component analysis (PCA) with DALI Z-scores. This analysis revealed three major structural super families (Groups 1, 2 and 3: Figure 5). Group-1 included AvrLm6 (kcl04-C) and AvrLm10A (kcl01-L) from *L. maculans* and SIX5 (kcl01-L) from *F. oxysporum,* but no KP6 proteins from *Zymoseptoria.* Group-2 contained Zt-KP6-4 (kcl02-D), ECP28-1/2 (kcl14-A), ECP28-3 (kcl14-B), BAS4 (kcl02-G), representatives of kcl01-C, kcl04-A, and kcl11-A, as well as UmV-KP6β. Group-3 was composed of Zt-KP6-1 (kcl06-B), UmV-KP6α, Zt-KP6-2 (kcl06-A), Zt-KP6-6 (kcl07-A), and a representative of kcl02-A. Taken together, this large-scale comparative structural analysis provided a first comprehensive description of the fungal KP6 effectors. In addition, it provided a reliable classification of the KP6 proteins into three major super families (groups in Figure 5) for follow-up studies.

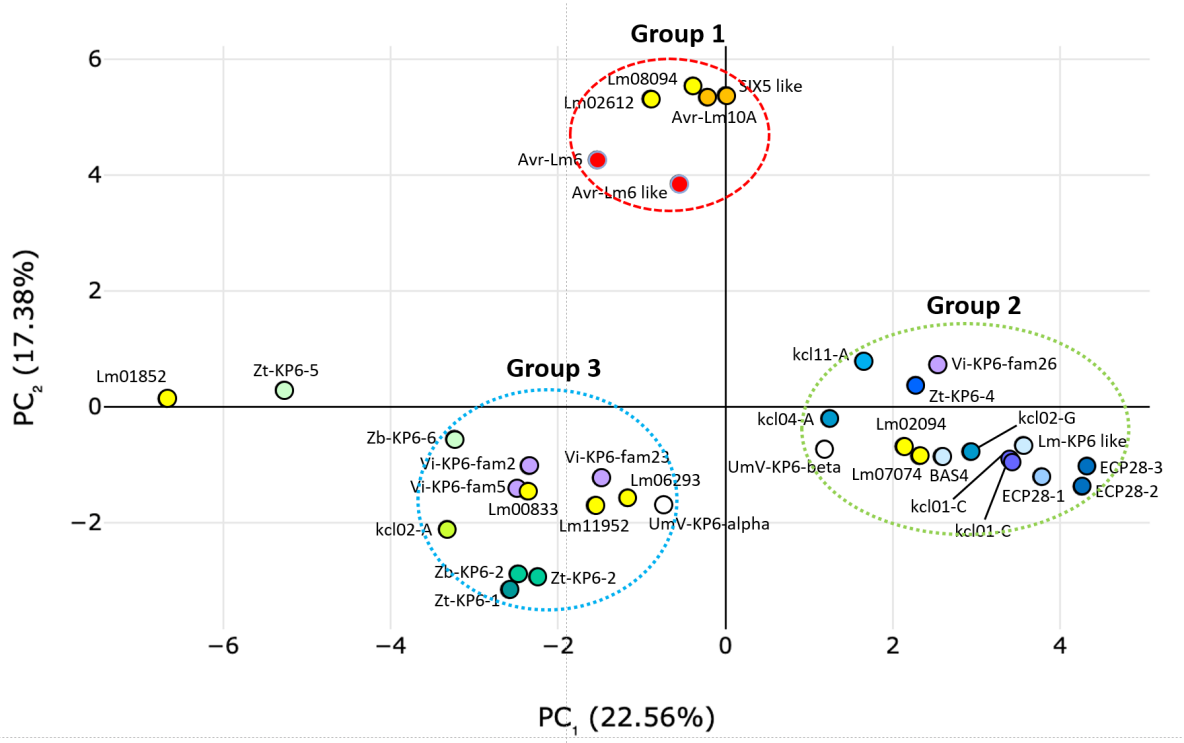

Figure 5 Classification of fungal KP6 according to their structures

DALI all by all analysis followed by a PCA using a DALI score matrix [28]. meta-cluster: kclXX, AFDB50 cluster: kclXX-Y, (number of proteins in the AFDB50 cluster), Uniprot number of the representative.

kcl01-C, (100), A0A4V3HRP1, M1W1H7; kcl01-L, (65), SIX5 = A0A010RIE2, AvrLm10A = E5A720_LEPMJ; kcl02-A, (5), A0A4R8TM13; kcl02-D, (138), Zt-KP6-4 = A0A2H1GZA7; kcl02-G, (321), A0A135SXI2; BAS4 = BAS4_MAGO7, Lm-KP6 = E5A0W1_LEPMJ; kcl04-A, (1), F9FAC2; kcl04-C, (25), AvrLm6 = A0A010QJV2;

366 *AvrLm6 = E5R515_LEPMJ; kcl06-A, (6), Zb-KP6-2 = A0A0F4GMG5, Zt-KP6-2 =*
367 *A0A2H1H0K4; kcl06-B, (3), Zt-KP6-1 = A0A2H1G421/6QKP; kcl07-A, (5), Zt-KP6-5 =*
368 *A0A2H1FMK1, Zb-KP6-6 = A0A0F4GGQ1; kcl11-A, (6), A0A317AKI4; kcl14-A, (93),*
369 *ECP28-2 = A0A1P8YXM1, ECP28-3 = A0A1P8YXM5; kcl14-B, (14), ECP28-1 =*
370 *A0A1P8YXQ5.*
371 *LmXXXX, Leptosphaeria KP6 proteins, (8 families), [15]; Vi-KP6-famXX, Venturia KP6*
372 *proteins, (4 families), [18]; White circle, UmV-KP6α, 4gvbA, White circle, UmV-KP6β,*
373 *4gvbB*
374
375 **KP4 proteins are abundant and widely distributed in fungi**
376
377 In addition to the HCE2 domain (PF14856) found in Zt-KP4-1, Zt-KP4-2 and Zt-KP4-3
378 [39], the pfam database comprises a KP4 domain (PF09044) initially defined by the
379 analysis of the *F. graminearum* proteins Fg-KP4-1, Fg-KP4-2 and Fg-KP4-3 related to
380 UmV-KP4. While the HCE2 domain relied on a pattern dominated by three conserved
381 cysteine and a W/F/Y motif, the KP4 domain was defined by a pattern involving four
382 conserved cysteine, three conserved glycine and two W/F/Y motifs [45,46].
383 Interestingly, we found no overlap in proteins retrieved from Uniprot with either the
384 HCE2 or the KP4 pfam domain. While the HCE2 domain was identified, as expected,
385 in Zt-KP4-1, Zt-KP4-2 and Zt-KP4-3, the KP4 domain was not identified in a
386 *Zymoseptoria* protein. To establish a comprehensive inventory of the KP4 proteins, we
387 searched 1014 fungal genomes with FHAT using Zt-KP4-1 and UmV-KP4 as
388 references (Sup Figure 9). We identified 4381 KP4 candidates grouped into 153
389 AFDB50 clusters that we merged into 44 FHAT meta-clusters. Visual inspection of the
390 structures of one representative protein from each meta-cluster rejected 31 meta-
391 clusters, which did not have the typical KP4 fold. The remaining 13 FHAT meta-clusters
392 gathered 3249 proteins with a KP4 fold (final KP4 FHAT database) including Ecp2
393 (kcl01), Zt-KP4-1 (kcl01), Zt-KP4-2 (kcl07), Zt-KP4-3 (kcl07), Zt-KP4-5 (kcl18), Zt-KP4-
394 6 (kcl09), Zt-KP4-7 (kcl09) and Zt-KP4-9 (kcl02) (sup Table 4). To search for structural
395 relationships among KP4 proteins, we selected at least one representative of each of
396 the 13 KP4 FHAT meta-clusters. This selection included known KP4 proteins such as
397 Fg-KP4-1 and Fg-KP4-2 which defined the KP4 pfam domain [45,46] and one Ecp2
398 (Paf-ECP2) used for defining the HCE2 pfam domain [39]. Additional known KP4
399 proteins such as Fg-KP4-3 [46], UmV-KP4 and two Ecp2 proteins (Sm-ECP2, Psf-ECP2)

400 used for the phylogenetic analysis of Zt-KP4-1 (Figure 4) were also selected. This
401 selection of 25 KP4 included all *Zymoseptoria* KP4 (Zt-KP4-1, 2, 3, 5, 6, 7, 9). The
402 similarity between the structures of these 25 proteins was assessed using a principal
403 component analysis (PCA) with DALI Z-scores. This analysis revealed four major
404 structural super families (Groups 1, 2, 3, 4: Figure 6). Group-1 was composed of Fg-
405 KP4-1, Fg-KP4-2 and Fg-KP4-3, UmV-KP4 and the representative of kcl02-A. Group-
406 2 contained Zt-KP4-1, Zt-KP4-2, Zt-KP4-3 and Ecp2 proteins, as well as the kcl07-A,
407 kcl10-A and kcl14-A representatives. Group-3 included the representatives of kcl08-A
408 and kcl38-A. Group-4 contained all other KP4 proteins, including Zt-KP4-5, Zt-KP4-6,
409 Zt-KP4-7 and Zt-KP4-9. Interestingly, all Group-1 proteins had a pfam KP4 domain,
410 while all proteins from Group-2 had an HCE2 domain. Proteins from Group-3 and
411 Group-4 did not have Pfam domains, with the exception of the representatives of kcl38-
412 A (PF15474) and kcl21-A (PF21691). This genome wide comparative structural
413 analysis provided a novel comprehensive inventory of plant and fungal KP4 proteins
414 that include the Ecp2 superfamilly. Their structure-based classification in four super
415 families (groups in Figure 6) clarified the relationship between proteins with either a
416 HCE2 or a KP4 pfam domain providing a novel framework for this large family of
417 effectors.
418

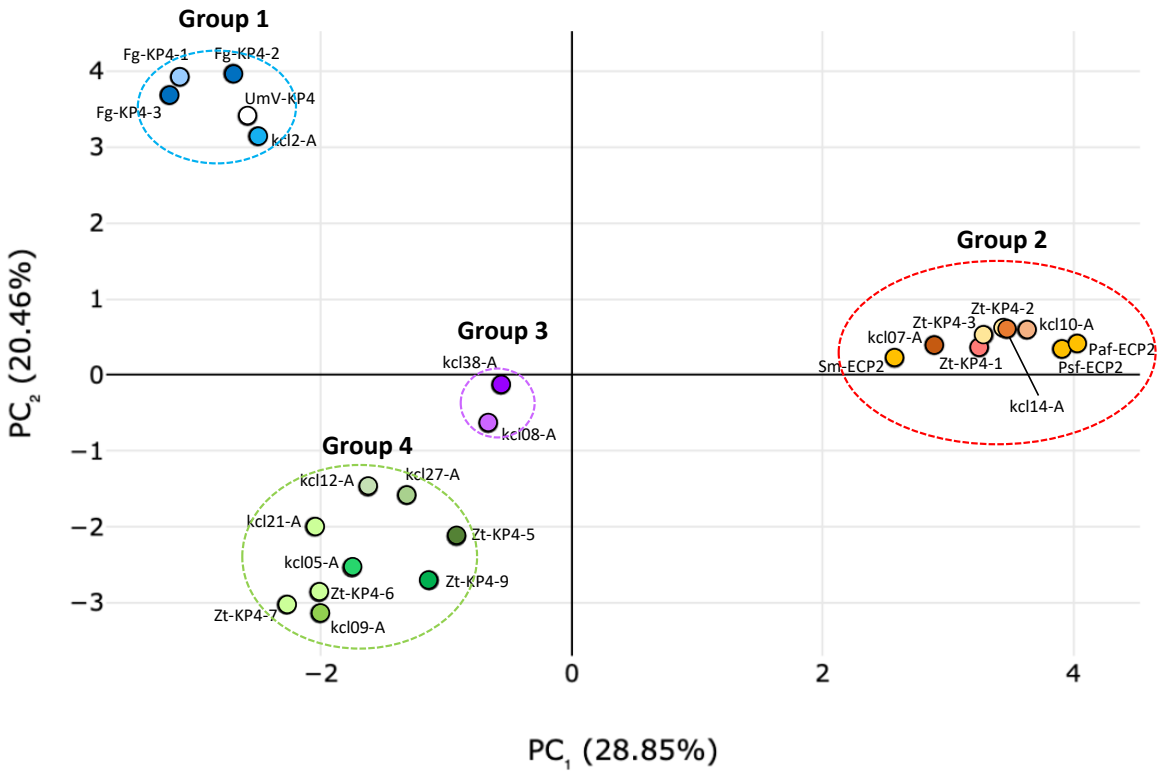

419

420

421 Figure 6 Classification of fungal KP4 families according to their structures

422 *DALI all by all analysis followed by a PCA using a DALI score matrix [28]. meta-cluster*
423 *kclXX, AFDB50 cluster kclXX-Y, (number of proteins in the AFDB50 cluster), Uniprot*
424 *number of the representative.*
425 *kcl01-D, (83), Zt-KP4-1 = A0A2H1H404/8ACX; kcl01-Q, (203), Sm-ECP2 = N1QK49,*
426 *Psf-ECP2 = M2Z6V3, Paf-ECP2 = Q00365; kcl02-A, (15), A0A4U0XEI9; kcl02-E,*
427 *(256), Fg-KP4-2 = A0A3S7E9S6, Fg-KP4-3 = A0A2H3GQS6; kcl02-I, (125), Fg-KP4-*
428 *1 = A0A2H3GK41; klc02-0, (324), Zt-KP4-9 = A0A2H1GXX1; kcl05-A, (14),*
429 *A0A6A6DAE0; kcl07-A, (53), A0A177DVW3; kcl07-C, (35), Zt-KP4-2 = A0A2H1FWY7;*
430 *Zt-KP4-3 = A0A1Y6M296; kcl08-A, (5), S3D5P; kcl09-A, (14), M3BT27; kcl09-B, (131),*
431 *Zt-KP4-6 = A0A2H1GNH3, Zt-KP4-7 = A0A2H1GND9; kcl10-A, (16), A0A1L9SH47;*
432 *kcl12-A, (9), E3L0Y8; kcl14-C, (12), A0A0A1V5R3; kcl18-A, (9), Zt-KP4-5 =*
433 *A0A2H1GP20; kcl21-A, (13), A0A0J9W663; kcl27-A, (39), A0A4T0WCM2; kcl38-A,*
434 *(8), A0A017SS08. White circle, UmV-KP4 = kptA*

435

436 **DISCUSSION**

437

438 The recent systematic investigation of the structures of fungal effectors revealed
439 extended protein families with conserved structures [5,20,21]. In this study, the
440 elucidation of the structure of two *Z. tritici* effectors (Zt-Mycgr3-91409-2, Zt-NIP1) by
441 X-ray crystallography revealed their unexpected structural similarity to the UmV-KP6α
442 and UmV-KP4 killer toxins from the dsRNA virus infecting the fungal pathogen *U.*
443 *maydis* [26]. Both effectors, renamed Zt-KP4-1 and Zt-KP6-1, were toxic to fungi, but
444 not to wheat. We established that proteins structurally related to Zt-KP4-1 and Zt-KP6-
445 1 are widespread and abundant in fungi, and belong to extended super families of
446 structurally related proteins. These results provided a novel comprehensive
447 classification of these effectors into, respectively, four KP4 and three KP6 super
448 families, providing a solid framework for studying these fascinating proteins.

449

450 ***UmV*-KP6 and *UmV*-KP4 killer toxins**

451

452 *U. maydis* secretes three killer proteins (UmV-KP1, KP4 and KP6) encoded by double-
453 stranded RNA viruses (UmV) [26,47,48]. They kill susceptible *U. maydis* strains, while

454 UmV-infected strains are resistant to the killer protein they produce [25,26]. UmV-KP4
455 inhibited fungal growth presumably by perturbing cellular calcium homeostasis [48],
456 and inhibited L-type voltage-gated (LVG) Ca^{2+} channels in mammalian cells [49].
457 Interestingly, UmV-KP4 also perturbed Ca^{2+} gradients of plant root hair cells [50]. The
458 *P. patrens* moss KP4 protein also modified Ca^{2+} gradients of moss cells [51]. However,
459 UmV-KP4 does not induce major growth defects, necrosis, chlorosis or cell death when
460 over-expressed in transgenic plants such as wheat, corn or tobacco [52–55]. UmV-
461 KP6α and UmV-KP6β associate to form a stable heterodimer [29]. UmV-KP6α appears
462 necessary for recognition of susceptible cells, through a mechanism involving the N-
463 terminal α helix, while UmV-KP6β is required for toxicity [26]. However, the molecular
464 mechanism underpinning the toxicity of UmV-KP6α/β to fungal cells is unknown [26],
465 although it has been hypothesised that this complex forms membrane pores [29].
466 These previous studies on KP4 and KP6 proteins provided interesting insights into their
467 function. However, a full understanding of their mode of action on plant and fungal cells
468 and their biological function is still lacking.
469
470 **Zt-KP6-1 and Zt-KP4-1 are antifungal proteins**
471
472 Neither Zt-KP4-1 nor Zt-KP6-1 induced necrosis when infiltrated into wheat leaves.
473 Similarly, Fg-KP4L-2 from *F. graminearum* did not induce necrosis of wheat leaves
474 [46]. Still, recombinant Fg-KP4L-2 slightly inhibited the growth of wheat roots [46]. This
475 is reminiscent of the low activity of UmV-KP4 on *A. thaliana* root growth [50]. We
476 showed that both Zt-KP4-1 and Zt-KP6-1 inhibited the growth of *Z. tritici* and *B. cinerea*.
477 Within *U. maydis*, UmV-KP4 and UmV-KP6 were only toxic to susceptible strains [26].
478 However, UmV-KP4 inhibited the growth of other fungi such as *Tilletia caries*, *Ustilago*
479 *tritici*, *Alternaria alternata* and *Phoma exigua* [54], but not the yeast *S. cerevisae* [56].
480 When overexpressed in transgenic wheat or tobacco, UmV-KP4 conferred resistance
481 to, respectively, *T. caries* and *U. tritici* [52,53,55], and *A. alternata* and *P. exigua* [54].
482 UmV-KP6 was also toxic to the yeast *Brettanomyces bruxellensis* [57], but not *S.*
483 *cerevisae* [47,57]. The structure-activity relationship of Zt-KP6-1 likely differs from
484 UmV-KP6α/β as it did not require the formation of a heterodimer to be toxic [26,29]. In
485 addition, Zt-KP6-1 does not have the N-terminal α-helical extension of UmV-KP6α
486 critical for its toxicity [26,29]. Since structural homologs of Zt-KP4-1 and Zt-KP6-1 are
487 widespread in fungi, it is tempting to speculate that other KP4 and KP6 proteins are

488 also toxic to fungi. Recent work on plant pathogenic fungi highlighted effectors with
489 antimicrobial activities [58]. For instance, the broad host range plant pathogenic fungus
490 *Verticiulium dahliae* secretes several effectors during host xylem invasion that have an
491 antibacterial activity [59]. These antimicrobial effectors changed the composition of the
492 xylem and root bacterial microbiota of host plants [60,61]. In particular, VdAve1, an
493 effector with antibacterial activity, specifically inhibits the growth of *Sphingomonas*
494 bacteria, which acts antagonistically toward *V. dahliae* in the host plant rhizosphere
495 [59,62]. AMAPEC, a machine-learning based computational software using shared
496 structural and physicochemical properties of known antimicrobial proteins, identified a
497 large number of candidate antimicrobial proteins among effectors of three different
498 plant-associated fungi [63]. This finding suggests that fungi have extended repertoires
499 of antimicrobial effectors. Most of KP4 and KP6 proteins identified in this study were
500 predicted to be antimicrobial according to AMAPEC (83% of KP6, 77% of KP4, Sup
501 Table 5), including Zt-KP4-1 and Zt-KP6-1. It will therefore be interesting to investigate
502 whether KP4 and KP6 super families are primarily composed of antimicrobial effectors.
503
504 **Fungal KP4 and KP6 proteins are widespread in fungi and define novel structural**
505 **super families with possible conserved functions**
506
507 To identify structural homologs of Zt-KP4-1 and Zt-KP6-1, we developed a novel
508 pipeline based on (i) FoldSeek structure similarity searches using AF2 structural
509 models of fungal secreted proteins, combined with (ii) HMM pattern searches relying
510 on Zt-KP4/UmV-KP4 or Zt-KP6/UmV-KP6α conserved cysteine patterns and (iii)
511 structure-based manual curation (FHAT, Sup Figure 9). In this last important step, the
512 topology and structure of KP4 and KP6 proteins were manually compared to Zt-
513 KP4/UmV-KP4 or Zt-KP6/UmV-KP6α. This procedure discriminated proteins with a
514 true KP4 or KP6 structural fold from proteins with limited or no structural similarity. To
515 assess the performance of FHAT, we compared our dataset with those of two recent
516 systematic structural studies of fungal effectors [20,21]. Clustering the KP4 and KP6
517 proteins identified in the three studies into families of highly related proteins (at least
518 90% sequence identity and 60% coverage) identified 1737 KP4 families for FHAT, 227
519 for Seong and 333 for Derbyshire, as well as 559 KP6 families for FHAT, 97 for Seong
520 and 80 for Derbyshire. The differences in the numbers of proteins identified mostly
521 come from large differences in the number of fungal genomes analyzed. We therefore

522 specifically compared these datasets for proteins detected in the seven shared fungal
523 species (Figure 7). Most KP4 and KP6 identified by FHAT in *Z. tritici* were also found
524 by Seong and/or Derbyshire (80%, Figure 7). However, FHAT was the only method
525 uncovering Zt-KP4-1, Zt-KP4-5 and Zt-KP6-6. Ten KP4 and two KP6 were specifically
526 detected by Derbyshire in *Z. tritici* (Figure 7). However, their structures did not display
527 the typical KP4 or KP6 fold, suggesting that these proteins were false positive. No false
528 positive were detected by Seong in *Z. tritici*. The same trend was observed for the six
529 other shared species (Figure 7). This result suggested that FHAT was more sensitive
530 than previous analyses, and has a low false positive rate. Consequently, it provides a
531 comprehensive inventory for these important effector families in fungi.
532
533 KP4 and KP6 proteins were found in both *ascomycotina* and *basidiomycotina* with
534 different lifestyles, including plant pathogens, plant symbionts and saprophytes, but
535 excluding as a notable exception animal fungal pathogen. Contrary to KP6 proteins,
536 KP4 proteins were identified outside fungi, in plants. Some plant KP4 clustered with
537 Fg-KP4 and UmV-KP4 in AFDB cluster kcl02-E from Group-1 (Figure 6), as observed
538 by Brown (2011), Lu and Faris (2019), and Guan (2023). Another set of plant KP4 (175
539 proteins) were related at the sequence level since they belonged to the same AFDB
540 cluster (kcl01-R) and they shared the same pfam domain (PF1657) characteristic of
541 plant antifungal proteins such as Ginkgobilobin-2.
542

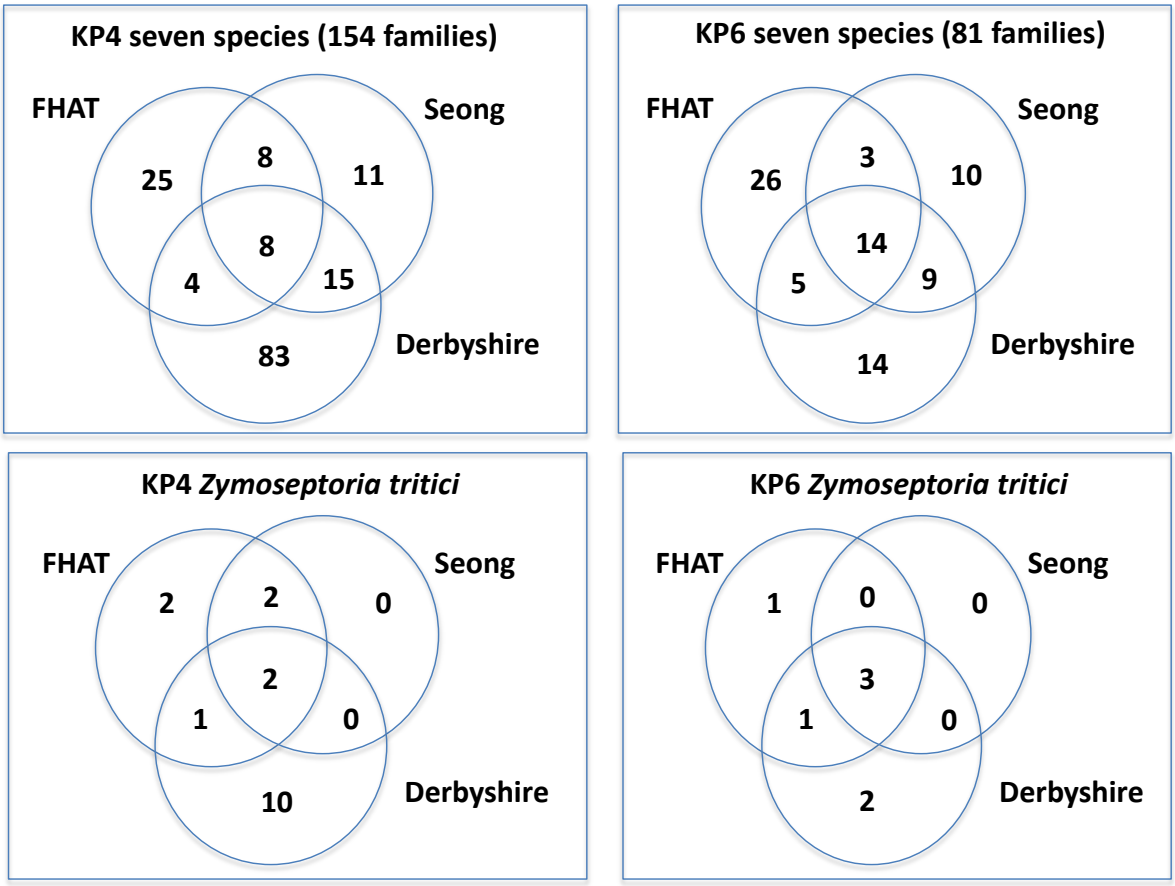

Figure 7. KP4 and KP6 proteins identified by FHAT and previous methods.

FHAT (Sup. Figure 10), Seong: [20], Derbyshire: [21]. KP4 and KP6 protein sequences found in the seven shared fungal species by the three methods, were clustered into highly related protein families sharing at least 90% sequence identity and 60% sequence overlap. The numbers of effector families detected by one or more methods are indicated in the Venn diagrams for KP4 and KP6 proteins of either the seven shared species or only Z. tritici. The seven shared species are: Blumeria graminis, Botryotinia fuckeliana, Fusarium oxysporum, Leptosphaeria maculans, Magnaporthe oryzae, Verticillium dahliae, Zymoseptoria tritici,

Our structure-based classification of the KP4 structural family integrated results from previous large-scale comparative studies and created a robust framework for future research (see Figure 6). KP4 structural Group-1 overlapped with the KP4 family characterized by the presence of a KP4 pfam domain defined using Fg-KP4 and UmV-KP4 by Lu and Faris (2019), and Brown (2011). KP4 structural Group1 contained 396 KP4 proteins from AFDB clusters kcl02-A, kcl02-E and klc02-I including 3 KP4 of the

561 moss *Physcomitrium patens* from kcl02-E [51]. KP4 structural Group-2 overlapped with
562 the Ecp2 family characterized by the presence of a HCE2 pfam domain [39]. KP4
563 structural Group-2 contained 402 proteins from the clusters kcl01-D, kcl01-Q, kcl07-A,
564 kcl10-A and kcl14-A. The discovery that KP4 and Ecp2 families are major groups of
565 the KP4 structural family is a novel finding generating far-reaching hypothesis on their
566 function and evolution. Combined with the finding that UmV-KP4 and Zt-KP4-1 from
567 structural Group-1 and -2 are toxic to fungi, we hypothesized that KP4 proteins from
568 these two structural groups are antimicrobial. Such effectors could be essential for the
569 competition of fungi during their colonization of particular ecological niches. This
570 hypothesis could be extended to Group-3 and -4 KP4 even though they neither
571 contained HCE2 or KP4 domains, nor have known biological function. The following
572 step will be to investigate the antimicrobial activity of a wide array of different KP4
573 proteins.
574
575 Our structure-based classification of the KP6 structural family provided a unifying
576 framework facilitating future research on these proteins (Figure 5). The KP6 structural
577 Group-1 included AvrLm10A and SIX5 that physically interact with effectors encoded
578 by neighbouring genes, facilitating their symplastic transport in host plant tissues
579 [14,16,64,65]. We hypothesized that his group, containing 25 fungal proteins from the
580 kcl04-C AFDB cluster but no proteins from *Zymoseptoria*, has evolved to act in the cell-
581 to-cell transport of other effectors [14]. The situation was different with proteins from
582 KP6 structural Group-2 and 3. KP6 structural Group-2 included the antifungal protein
583 UmV-KP6β, the known effectors BAS4 from *P. oryzae* [43] and ECP28 from *P. fulvum*
584 [42], Zt-KP6-4, and 420 KP6 proteins from clusters kcl01-C, kcl02-G, kcl04-A and
585 kcl11. Similarly, KP6 structural Group-3 contained the two antifungal proteins Zt-KP6-
586 1 and UmV-KP6α, as well as Zt-KP6-2, Zt-KP6-6, and five KP6 proteins from cluster
587 kcl02-A. We hypothesized that these two KP6 structural Groups could gather proteins
588 with antimicrobial activity. Testing this hypothesis will require the investigation of the
589 antimicrobial activity of a wide array of KP6 proteins.
590
591

592 MATERIELS AND METHODS

593

594 **Protein expression and purification**

595 The Zt-KP6 mature protein (residues 21-90) was expressed with the pET-SP vector,
596 produced and purified as previously described [5]. The Zt-KP4 protein was expressed
597 with the pET derived plasmid pdbccdb-3C-His, produced and purified as previously
598 described [7] (Supplementals File S1) .

599

600 **Nuclear magnetic resonance spectroscopy**

601 To generate isotopically labelled samples for NMR spectroscopy, we used $^{15}NH_4Cl$, as
602 the unique source of nitrogen. The samples containing 0,7 mM of purified protein in
603 10 % D_2O and 1 µM DSS as a reference were analyzed using an 800 MHz Avance
604 Bruker spectrometer and a TCI probe at 303 K. Spectra were recorded with Topspin
605 3.2 (Bruker) and referenced to DSS (4,4-dimethyl-4-silapentane-1-sulfonic acid) for the
606 ^{1}H dimension and indirectly for the ^{15}N dimension. NMR data were processed using
607 Topspin 3.6 (Bruker) and analyzed with the in-house software Cindy 2.1 (Padilla,
608 www.cbs.cnrs.fr). Side chain assignments were carried out using 2D-NOESY, 2D-
609 TOCSY and COSY-DQF experiments with D_2O samples, combined with ^{15}N-NOESY-
610 HSQC and ^{15}N-TOCSY-HSQC 3D spectra. The CYANA 3 program [66] was used for
611 automatic NOE assignments and structure calculations. The CANDID procedure of
612 CYANA was used to assign the 3D-peaks list from the ^{15}N-NOESY-HSQC spectra.
613 Structures were analyzed with PROCHECK [67]. Refinement statistics for the structure
614 are listed in Sup. Table 1. The structure of Zt-KP6 was deposited in the Protein Data
615 Bank and in BMRB with accession number 9GWD and ID 34963 respectively.

616

617 **X-ray crystallography**

618 The purified protein Zt-KP6 was concentrated to 10 mg/ml in 20 mM Tris-HCl, pH 8.0,
619 150 mM NaCl, 1 mM DTT. The purified protein Zt-KP4 was concentrated to 8 mg/ml in
620 20 mM NaCi, pH 5.6, 150 mM NaCl, 1 mM DTT. Crystallization trials were performed
621 at 20°C by the hanging-drop vapor-diffusion method in 96-well microplates using a
622 Mosquito HTS robot with 100 nl of protein mixed with 100 nl of reservoir. After 3 weeks,
623 Zt-KP6 crystals were obtained from the condition 0.01 M $NiCl_2$, 0.1 M Tris pH 8.5, 1M
624 $LiSO_4$ (from classic kit, Hampton research®). After refinement and soaking in tantalum,
625 diffraction crystals were obtained in 0.1M Tris pH 9, 1.5M $LiSO_4$, 100mM $ZnSO_4$. After

626 2 weeks, small crystals of Zt-KP4 were obtained from one condition of the Peg kit
627 (Qiagen®) containing 0.1M sodium acetate pH 4.6 and 30%(v/v) PEG 300. All crystals
628 were flash frozen in liquid nitrogen.
629
630 **Data collection, processing and structure determination**
631 Crystal diffraction datasets were collected at the European Synchrotron Radiation
632 Facility (ESRF, Grenoble). For Zt-KP6, data were collected at beam line ID30A-1 [68–
633 72] using a Pixel detector (Pilatus3-2M) and processed by XDS [73] and AIMLESS
634 [74], from the CCP4/CCP4i programs suite [75,76]. For Zt-KP4, data were collected
635 at beam line ID30B [77,78] using a Pixel detector (PILATUS3 6M) and auto processed
636 by XDSAPP [79,80]. Zt-KP6 crystals belong to the $P2_12_12_1$ space group and contain
637 two molecules in the asymmetric unit. The structure of Zt-KP6 was determined to 1.36
638 Å by the single wavelength anomalous diffraction (SAD) method using HKL2MAP
639 [81,82]. Zt-KP4 crystals belong to the H3 space group and contain eight molecules in
640 the asymmetric unit. The structure of Zt-KP4 was determined by molecular
641 replacement with Molrep [83] from CCP4I2 [76] using the model determined by AF2
642 [19]. After modelbuilding using arp/warp [84], Coot [85] and refinement by REFINE
643 from PHENIX [86,87] final structures had R(%) / R(%)free of 14 / 18.3 for Zt-KP6 and
644 17.5 / 21.9 for Zt-KP4. Data collection and refinement statistics for the structures are
645 listed in Sup. Table 2. Figures were generated using PyMol v1.6
646 (http://www.pymol.org/). The atomic coordinates and structure factors of Zt-KP6 and
647 Zt-KP4, were deposited in the Protein Data Bank with accession numbers 6QPK and
648 8ACX respectively.
649
650 **Biological assays of Zt-KP4-1 and Zt-KP6-1**
651 Zt-KP4-1 and Zt-KP6-1 were infiltrated into leaves of the wheat cultivar Taichung 29 at
652 a concentration of 2 µM. As a control, the necrotrophic effector ToxA from *P. nodorum*
653 [33] was infiltrated into Taichung 29 wheat leaves at concentrations from 0.2 to 2 µM.
654 *Z. tritici* IPO323 isolate and the necrotrophic plant pathogen *Botrytis cinerea* were used
655 for growth assays in 96 well microtiter plates containing liquid potato dextrose growth
656 medium (PDA). Each well of the plate was filled with 100µL of PDA containing either
657 10E6 *Z. tritici* spores/mL or 10E6 *B. cinerea* spores/mL and different concentrations of
658 Zt-KP4-1 or Zt-KP6-1 (0.55, 1.65 and 5.5 µM). 96 well plates were incubated in the
659 dark at either 18°C (*Z. tritici*) or 25°C (*B. cinerea*) with shaking (50 rpm). After 7 days

660 of growth, the OD at 580 nm was recorded on a spectrophotometer. The % of inhibition
661 was calculated according to the formula: % inhibition = ((OD treated/OD control)-
662 1)*100. Values displayed in Table 1 were the mean ± Standard Error Deviation (SED)
663 from three independent experiments.
664
665 **FHAT protocol for the detection of fungal KP4 and KP6 proteins**
666 Fungal KP4 and KP6 proteins were retrieved from public databases according to the
667 following protocol (Sup Figure 9) and result files for each step are available at URLs
668 https://pat.cbs.cnrs.fr/kp4/fhat_kp4 and https://pat.cbs.cnrs.fr/kp6/fhat_kp6. The
669 protocol for the detection of fungal KP4 and KP6 proteins is fully described in the
670 legend of Sup Figure 9.
671
672 **PCA analysis**
673 To classify KP4 and KP6 proteins according to their structural similarities, an ”all
674 against all” analysis was performed for both families using the DALI server [28]. This
675 computing delivered matrices of all the Z-scores for each pair of proteins. If a pair of
676 proteins had a Z-score of 0.1, they were excluded from the following step. A Principal
677 Component Analysis (PCA) was performed using these Z-scores matrices using
678 *Statistic Kingdom* (https://www.statskingdom.com/410multi_linear_regression.html).
679 Protein names were directly labeled on the graphs.
680
681 **Acknowledgements**
682 The CBS is a member of the French Infrastructure for Integrated Structural Biology
683 (FRISBI), national infrastructure supported by the French National Research Agency
684 (ANR-10-INBS-0005). We thank R. Lambert for assistance with protein production and
685 x-ray crystallography. We are grateful to Matthew Bowler and Didier Nurizzo at the
686 European Synchrotron Radiation Facility (ESRF), Grenoble, France for providing
687 assistance in using beamline ID30B and ID30A-1 and the ESRF for provision of
688 synchrotron radiation facilities via Block Allocation Group beamtime.
689
690 **Data availability**
691
692 The data that support the findings of this study are openly available at the following
693 URLs:

https://pat.cbs.cnrs.fr/kp4/fhat_kp4

https://pat.cbs.cnrs.fr/kp6/fhat_kp6

Authors contributions

KDG, AP, TK and MHL planned and designed the research. KDG, LM, JG, PB, FH, ML, JR, YPH and MHL performed experiments and analysed data. KDG, AP, TK and MHL wrote the manuscript.

List of figures and table:

Figure 1. ***Crystal structures of (A) Zt-KP6-1 (6QPK chain A) and (B) UmV-KP6α (4GVB chain A).***

(A) Zt-Mycgr3-91409-2 was renamed to Zt-KP6-1 according to its structural homology to UmV-KP6α (see text). Structures were coloured in rainbow colours from blue (N terminus) to red (C terminus). For Zt-KP6-1, the loop connecting β1 (in blue) to H1 (in cyan) was not observed in the density map and is shown as a blue dashed line. Disulphide bonds are shown in grey and labelled Dx. For the D1 (C26-C86) bond in Zt-KP6-1, both conformations are shown.

Figure 2. Crystal structures of (A) Zt-KP4-1 (8ACX chain A) and (B) UmV-KP4 (1KPT chain A).

(A) Zt-NIP1 was renamed to Zt-KP4-1 according to its structural similarity to UmV-KP4 using DALI (see main text). Structures were coloured in rainbow colours from blue (N terminus) to red (C terminus). For Zt-KP4-1 the loops connecting β6 to β7 and β6 to H1 were not observed in the density map and were shown as dashed lines. Disulphide bonds are shown in grey and labelled Dx.

Figure 3. Phylogenetic tree of *Zymoseptoria* KP6-1 and KP6-2

MAFFT alignment, BMGE cleaning, PhyML Phylogenetic tree using NGPhylogeny.fr. [37] Bootstrap values > 70% are indicated under each branch after the supported node. Midpoint tree rooting. Zt-KP6-1_Ztritici_3D7: Uniprot A0A1X7RM13 (identical to Zt-KP6-1_IPO323); Zt-KP6-1_Ztritici_1E4: Uniprot A0A2H1G421, PDB 6QKP; Zp-KP6-1_Zpseudotritici: JGI Zymps1_802032; Zt-KP6-2_Ztritici_1E4: Uniprot A0A2H1H0K4; Zt-KP6-2_Ztritici_IPO323: Uniprot F9XLY9; Zt-KP6-2_Ztritici_3D7: Uniprot A0A1X7S5L2; Zb-KP6-2_Zbrevis: Uniprot A0A0F4GMG5; Za-KP6-2_Zardabiliae: JGI Za_774343 ; Zp-KP6-2_Zpseudotritici: JGI Zymps1_805921.

Figure 4. Phylogenetic tree of *Zymoseptoria* KP4-1, KP4-2, and KP4-3

MAFFT alignment, BMGE cleaning, PhyML Phylogenetic tree using NGPhylogeny.fr [37]. Bootstrap values > 70% are indicated under each branch after the supported node. Tree root with Ecp2_Passalora fulva and Ecp2_Pseudocercospora fijiensis as

736 outgroups. Zt-KP4-1_Ztritici_IPO323: re-annotated NIP1/Mycgr3-106176 see Sup.
737 Fig1; Zt-KP4-1_Ztritici_1E4: Uniprot A0A2H1H404; Zt-KP4-1_Ztritici_3D7: Uniprot
738 A0A1X7S6U3; Zt-KP4-1_Ztritici_1A5: Uniprot A0A1Y6M012; Zt-KP4-
739 2_Ztritici_IPO323: Mycgr3-107904, Uniprot F9X223; Zb-KP4-2_Zbrevis: KJY02238,
740 Uniprot A0A0F4GYX0; Zt-KP4-3_Ztritici_IPO323: Mycgr3-111636, Uniprot F9XQ02;
741 Zt-KP4-3_Ztritici_3D7: Uniprot A0A1X7S9R6; Zb-KP4-3_Zbrevis: KJX96086, Uniprot
742 A0A0F4GF74; Ecp2_Passalora fulva: Uniprot Q00365; Ecp2_Pseudocercospora
743 fijiensis: Uniprot M2Z6V3; Ecp2_Sphaerulina musiva: Uniprot N1QK49;
744 Ecp2_Cochliobolus sativus: Uniprot M2TE34
745
746 **Figure 5. Classification of fungal KP6 families according to their structures**
747 DALI all by all analysis followed by a PCA using a DALI score matrix [28]. meta-cluster:
748 kclXX, AFDB50 cluster: kclXX-Y, (number of proteins in the AFDB50 cluster), Uniprot
749 number of the representative.
750 kcl01-C, (100), A0A4V3HRP1, M1W1H7; kcl01-L, (65), SIX5 = A0A010RIE2,
751 AvrLm10A = E5A720_LEPMJ; kcl02-A, (5), A0A4R8TM13; kcl02-D, (138), Zt-KP6-4 =
752 A0A2H1GZA7; kcl02-G, (321), A0A135SXI2; BAS4 = BAS4_MAGO7, Lm-KP6 =
753 E5A0W1_LEPMJ; kcl04-A, (1), F9FAC2; kcl04-C, (25), AvrLm6 = A0A010QJV2;
754 AvrLm6 = E5R515_LEPMJ; kcl06-A, (6), Zb-KP6-2 = A0A0F4GMG5, Zt-KP6-2 =
755 A0A2H1H0K4; kcl06-B, (3), Zt-KP6-1 = A0A2H1G421/6QKP; kcl07-A, (5), Zt-KP6-5 =
756 A0A2H1FMK1, Zb-KP6-6 = A0A0F4GGQ1; kcl11-A, (6), A0A317AKI4; kcl14-A, (93),
757 ECP28-2 = A0A1P8YXM1, ECP28-3 = A0A1P8YXM5; kcl14-B, (14), ECP28-1 =
758 A0A1P8YXQ5.
759 LmXXXX, Leptosphaeria KP6 proteins, (8 families), [15]; Vi-KP6-famXX, Venturia KP6
760 proteins, (4 families), [18]; White circle, UmV-KP6α, 4gvbA, White circle, UmV-KP6β,
761 4gvbB
762
763 **Figure 6. Classification of fungal KP4 families according to their structures**
764 DALI all by all analysis followed by a PCA using a DALI score matrix [28]. meta-cluster
765 kclXX, AFDB50 cluster kclXX-Y, (number of proteins in the AFDB50 cluster), Uniprot
766 number of the representative.
767 kcl01-D, (83), Zt-KP4-1 = A0A2H1H404/8ACX; kcl01-Q, (203), Sm-ECP2 = N1QK49,
768 Psf-ECP2 = M2Z6V3, Paf-ECP2 = Q00365; kcl02-A, (15), A0A4U0XEI9; kcl02-E,
769 (256), Fg-KP4-2 = A0A3S7E9S6, Fg-KP4-3 = A0A2H3GQS6; kcl02-I, (125), Fg-KP4-

770 1 = A0A2H3GK41; klc02-0, (324), Zt-KP4-9 = A0A2H1GXX1; kcl05-A, (14),
771 A0A6A6DAE0; kcl07-A, (53), A0A177DVW3; kcl07-C, (35), Zt-KP4-2 = A0A2H1FWY7;
772 Zt-KP4-3 = A0A1Y6M296; kcl08-A, (5), S3D5P; kcl09-A, (14), M3BT27; kcl09-B, (131),
773 Zt-KP4-6 = A0A2H1GNH3, Zt-KP4-7 = A0A2H1GND9; kcl10-A, (16), A0A1L9SH47;
774 kcl12-A, (9), E3L0Y8; kcl14-C, (12), A0A0A1V5R3; kcl18-A, (9), Zt-KP4-5 =
775 A0A2H1GP20; kcl21-A, (13), A0A0J9W663; kcl27-A, (39), A0A4T0WCM2; kcl38-A,
776 (8), A0A017SS08. White circle, UmV-KP4 = kptA
777
778 **Figure 7. KP4 and KP6 proteins identified by FHAT and previous methods.**
779 FHAT (Sup. Figure 10), Seong: [20], Derbyshire: [21]. KP4 and KP6 protein sequences
780 found in the seven shared fungal species by the three methods, were clustered into
781 highly related protein families sharing at least 90% sequence identity and 60%
782 sequence overlap. The numbers of effector families detected by one or more methods
783 are indicated in the Venn diagrams for KP4 and KP6 proteins of either the seven
784 shared species or only *Z. tritici*. The seven shared species are: *Blumeria graminis*,
785 *Botryotinia fuckeliana, Fusarium oxysporum, Leptosphaeria maculans, Magnaporthe*
786 *oryzae, Verticillium dahliae, Zymoseptoria tritici.*
787
788 **Table1. Toxicity of Zt-KP4-1 and Zt-KP6-1 to fungi**
789 The percentages of *B. cinerea* and *Z. tritici* growth inhibition were calculated for
790 different concentrations of ToxA, Zt-KP4-1and Zt-KP6-1. Values are the mean ±
791 Standard Error of the Mean (SEM) from three experiments.
792
793
794

795 **List of supplementary figures and tables:**

796

797 **Supplementary Figure 1. Annotation of IPO323 *Z. tritici* Zt-Mycgr3-91409 (Zt-KP6-**
798 **1) and Zt-Mycgr3-106176 (Zt-KP4-1)**

799 Sup. Fig.1-A Annotation of IPO323 *Z. tritici* CDS Zt-Mycgr3-91409 (Zt-KP6-1)

800 Sup. Fig.1-B Annotation of IPO323 *Z. tritici* CDS Zt-Mycgr3-106176 (Zt-KP4-1)

801

802 **Supplementary Figure 2 Purification of Zt-KP6-1 by gel filtration**

803 Gel filtration profile with a Superdex S75 26/60 (GE Healthcare) column at 2.5 ml/min
804 in buffer (20 mM Tris-HCl, pH 8.0, 150 mM NaCl, 1 mM DTT) and SDS-PAGE analysis
805 of purified Zt-KP6-1. Sizes of the molecular mass markers are indicated on the left of
806 the gel.

807

808 **Supplementary Figure 3 NMR analysis of Zt-KP6-1**

809 HSQC spectra of Zt-KP6-1 at, 0.7 mM in 20 mM NaCitrate pH 5.4, 150 mM NaCl, 1
810 mM DTT, 303 K, 800 MHz. Cross-peak assignments are indicated using one-letter
811 amino acid and number (the asterisk shows a folded red peak). Missing residue N36.

812

813 **Supplementary Figure 4 Topology diagrams of Zt-KP6-1 and UmV-KP6α**

814 The structures were processed by PDBsum and the secondary structures were colored
815 from N-terminus (blue) to C-terminus (red) according to Figure 1. Disulphide Bonds (D)
816 are represented as grey lines. The disulphide pattern of the UmV-KP6 proteins starts
817 with a CxC cysteine motif in β1 bound to cysteine residues in, respectively, β4 and H2
818 (equivalent to H1 in ZtKP6-1). The first cysteine in the β1 CxC motif and the linked
819 cysteine in β4 were missing in Zt-KP6-1 without affecting the antiparallel arrangement
820 of β4 and β1.

821

822 **Supplementary Figure 5 Purification of Zt-KP4-1 by gel filtration**

823 Gel filtration profile with a Superdex S75 16/60 (GE Healthcare) column at 1 ml/min in
824 buffer (20 mM NaCi, pH 5.6, 150 mM NaCl, 1 mM DTT) and SDS-PAGE analysis of
825 purified Zt-KP4-1. (a) dimer, (b) monomer. Sizes of the molecular mass markers are
826 indicated on the left of the gel.

827

828 **Supplementary Figure 6 Dimer of Zt-KP4-1 between chains B (cyan) and G (blue)**

829 Residues involved in hydrogen bonds at the dimer interface are labelled and
830 represented by sticks. Hydrophobic residues involved in the pocket are highlighted in
831 lines and coloured in yellow. According to the GenBank sequence SMR60557.1, the
832 residue numbering must start after the signal peptide at residue S20. T33 in the
833 structure corresponds to T48 in the GenBank sequence. Binding is mediated by four
834 hydrogen bonds between the Thr48, Ser50, Gln90, and Thr158 from chain E, G, F or
835 C and Thr158, Gln90, Ser50 and Thr48 from chain H, B, C or A respectively, as well
836 as a hydrophobic pocket formed by residues Val62 and Val149 of both chains.
837
838 **Supplementary Figure 7 Topology diagrams of Zt-KP4 and UmV-Kp4**
839 The structures were processed by PDBsum and the secondary structures were
840 coloured from N-terminus (blue) to C-terminus (red) according to the Figure 2.
841 Disulphide Bonds (D) are represented as grey lines. For UmV-KP4, the five disulphide
842 bonds were located between Cys5 in the N-terminus and Cys78 at the end of helix H3,
843 between Cys11 in H1 and Cys81 just before the start of β5, between Cys27 in H2 and
844 Cys67 in H3, between Cys35 at the end of β1 and Cys60 at the start of β4 and finally
845 between Cys44 at the end of β2 and Cys105 at the C-terminus (Figure 2). In their
846 study, Gage et al. (2002) reported that changing Lys42 of UmV-KP4 to glutamine
847 reduced KP4 biological activity by 90%. In Umv-KP4, Lys42 stabilised the disulphide
848 bridge involving Cys44 and Cys105 and it was proposed to be required for the stability
849 of the C-terminus (Gage et al. 2002). In Zt-NIP1, there was no amino acid involved in
850 stabilizing the C-terminus and the amino acid corresponding to Lys42 was replaced by
851 Thr85. However, the C-terminus of Zt-NIP1 was stabilised by the β7 strand.
852
853 **Supplementary Figure 8 Structure and topology of Zt-KP6-1 and Zt-KP6-2**
854 Zt-KP6-2 structure was predicted by AlphaFold2. The structures were processed by
855 PDBsum and the secondary structure were coloured from N-terminus (blue) to C-
856 terminus (red) according to Figure 1.
857
858 **Supplementary Figure 9 Flow chart of the pipeline used to identify fungal**
859 **proteins structurally related to Zt-KP6-1 and Zt-KP4-1**
860 - Step 1: Selection of the reference templates (result file1): First, PDB structures were
861 selected as reference templates for the validation of candidate 3D folds (1KPT-A and
862 8ACX-A in the case of KP4, 4GVB-A and 6QPK-A in the case of KP6).

863 - Step 2-1: Foldseek search (result files 2 and 4): AlphaFold2 models similar to the
864 reference PDB templates were detected in the AFDB50 database using the Foldseek
865 server (van Kempen et al. 2024).
866 - Step 2-2: The fungal representatives of the AFDBcluster database (Barrio-Hernandez
867 et al. 2023) were collected (result file 6) if they shared a Foldseek E-value below 1e-3
868 with any hit from the previous Foldseek search.
869
870 Output 1: AFDB50 cluster representatives corresponding to the KP4 and KP6
871 candidate proteins detected by Foldseek and AFDBcluster database.
872
873 - Step 3: Hmmer search (result file 3 and 5): The KP4 and KP6 proteins detected by
874 Foldseek in step 2-1, whose TM scores were above 0.5 were aligned according to
875 TMalign output. The resulting multiple sequence alignment was used as input query to
876 search for homologous sequences shorter than 300 residues using 10 Hmmer
877 iterations with E-value<1 and query overlap >75% in a custom fungal secretome
878 database. This custom database was composed of 713,879 secreted fungal proteins
879 which were predicted using SignalP 5.0 (Almagro Armenteros et al. 2019) from
880 9,785,231 protein sequences originating from 1014 annotated fungal genomes
881 available at the Ensembl web site (ftp.ensemblgenomes.org release-46).
882
883 Output 2: AFDB50 cluster representatives corresponding to the KP4 and KP6
884 candidate proteins detected by Foldseek and Hmmer.
885
886 - Step 4-1: Filtering (result file 8): The representatives of the AFDB50 clusters covering
887 all candidate proteins detected at both Step 2 (Output-1, Foldseek) and Step 3 (Output-
888 2, Hmmer) were selected if they were not predicted as transmembrane and if their
889 sequences were shorter than 180 residues. The members not predicted as secreted
890 by SignalP 5.0 were removed (Almagro Armenteros et al. 2019).
891 - Step 4-2: Structural validation (result files 9 to 12): The AlphaFold2 models of all the
892 representatives of the selected AFDB50 clusters, were validated if their TM-score was
893 above 0.5 when superposed by TMalign onto one the reference templates (Zhang et
894 Skolnick 2005). The TMscore cutoff was set at a rather high value of 0.5 to minimize
895 the detection of false positives.
896

897 Output-3: Members and representatives of the KP4 and KP6 AFDB50 clusters (kclX-
898 Y) filtered using Step4 criteria. Members = result file 18, Representatives = result file
899 13
900 - Step 5: Structural alignment (result file 15 and 16): Representatives of KP4 and
901 KP6 AFDBclusters were structurally aligned using TMalign onto a reference PDB
902 template, respectively on chain A of the PDB structure 1KPT for KP4, and on chain A
903 of the PDB structure 4GVB for KP6. Protein secondary structures were added at the
904 end of each alignment. Same as Step 4.3: Phylogeny (result file 17): Phylogenetic
905 trees of Representatives of KP4 and KP6 AFDBclusters were constructed using
906 FastME (Lefort, Desper, et Gascuel 2015) using structural alignments after removing
907 the aligned positions with more than 50% indels. Taxonomic information was suffixed
908 to each protein identifier.
909
910 - Step 6: Uniprot annotations analysis (result file 19 and 20): The most frequent Uniprot
911 annotations (UniProt Consortium, 2023) and the taxonomic distributions of the two
912 validated member sets were computed for further analysis. Annotations were listed in
913 a web page hyper-linked to external databases for an easy analysis of the proteins
914 whose domains, structures, orthologous groups or functions are already known. A
915 subset analysis was performed (result file 34 to 38): The most frequent Uniprot / Pfam
916 annotations of the protein subsets were collected. The AlphaFold2 models of each
917 subset protein was aligned using TMalign onto 8ACX for the KP4 like subset and 6QPK
918 for the KP6 like proteins. FastME trees were derived from these structural alignments
919 after the removal of their aligned positions with more than 50% indels. Known Pfam
920 family identifiers were suffixed to each protein identifier in the last result tree. Lastly,
921 each pair of selected 3D models was superposed using TMalign and a structural tree
922 was inferred from the obtained TM-scores using FastME. This tree was compared with
923 a phylogenetic tree derived from the corresponding multiple sequence alignment built
924 using MAFFT.
925
926 - Step 7: *Zymoseptoria* analysis (result file 22 to 24): The KP4 like and KP6 like
927 detected in *Zymoseptoria* were superposed onto experimental structures 8ACX and
928 6QKP. The TMscores of each superposition were collected and phylogenetic trees
929 were inferred using TMalign from both *Zymoseptoria* alignments without the columns
930 with more than 50% indels.

931

932 - Step 8: Comparison of the final set to previous studies (result file 25 and 26): The
933 detected KP4 like set was compared to those detected in previous studies on fungal
934 effectors (Seong et Krasileva 2023; Derbyshire et Raffaele 2023). By using Kclust
935 (Hauser, Mayer, et Söding 2013), the validated KP4 like proteins were clustered with
936 the KP4 proteins detected by the other studies if their sequences shared more than
937 30% sequence identity and more than 80% sequence overlap. The diversity of the KP4
938 like protein set detected by each method was estimated as the percentage of the above
939 30%id-max clusters which include at least one protein. The same clustering analysis
940 was done for the KP6 proteins.

941

942 - Step 9: K-clust Clustering (result file 29 to 33): We have clustered all the proteins
943 from Step 4 (Representatives of the selected KP4 and KP6 AFDBclusters) using
944 Kclust at 40% maximum shared sequence identity. Meta-clusters (kclX) were
945 selected by a hierarchical clustering of the representatives which share more than
946 40% identical positions between both their amino acid sequences and their
947 secondary structures coded as 3-classe sequences (H for helix, E for extended
948 strand, C for coil).

949

950 - Step 10: Final structural validation. The structures of the proteins representative of
951 each meta-cluster from Step 5 (kcl-X) were predicted by AlphaFold2. If the
952 representative of the meta-cluster displayed a pLDDT score below 50, another
953 member of the same meta-cluster with pLDDT above this value was used.

954

955 The topology of each KP4 representative was visually inspected with Pymol, and it
956 was validated or rejected as a KP4 according to following topology: H2-β1-β2-β3-β4-
957 H3-β5-β6. The first 15 N-terminal residues were not taken into account. To be
958 validated the candidate protein must display two antiparallel alpha-helices H2 and
959 H3. The two antiparallel strands β1 and β4 were sometime poorly defined, since
960 these two strands were short and their arrangement difficult to confirm. Strands β2
961 and β3 must be present. However, β2 was sometime replaced by an alpha-helix. The
962 presence of the antiparallel strands β5 and β6 as well as β6-β3 and their proximity
963 must be present. Candidate KP4 proteins that do not meet these criteria were
964 eliminated from further consideration.

965
966 The topology of each KP6 representative was visually inspected with Pymol, and
967 it was validated or rejected as a fold according to following topology: H2-β1-β2-
968 β3-β4-H3-β5-β6. The validation of a KP6 fold required the following topology: β1-
969 H2-β2-β3-H3-β4. The KP6 fold required for validation was defined according to
970 the following topology: β1-H2-β2-β3-H3-β4. The short N-terminal H1 helix does
971 not play a role in determining the core topology, and it was not taken into account.
972 The two antiparallel helices H2 and H3 were detected in the structure of all the
973 selected KP6 meta-cluster representatives. To be validated the candidate protein
974 must display antiparallel strands β1, β3 and β4 with β1 strand central and in
975 antiparallel arrangement with β3 and β4. The two antiparallel strands β2 and β3
976 must be present and H3 must be connected to β4. Overall, the β sheet formed by
977 β1-β2-β3-β4 must be observed on one side (sometimes with poorly defined
978 strands) and the two helices H2 and H3 on the other side. Candidate KP6
979 proteins that do not meet these criteria were eliminated from further consideration.
980
981 - Step 11: Final members and representatives of KP4 or KP6 clusters
982 The result file(s) of each analysis step are displayed for both KP4 and KP6 protein
983 families at the following URLs:
984 - https://pat.cbs.cnrs.fr/kp4/fhat_kp4
985 - https://pat.cbs.cnrs.fr/kp6/fhat_kp6
986
987 **Supplementary Figure 10 Structure and topology of Zt-KP4-1, Zt-KP4-2 and Zt-**
988 **KP4-3**
989 Zt-KP4-2 and Zt-KP4-3 structures were predicted by AlphaFold2. The structures were
990 processed by PDBsum and the secondary structures were coloured from N-terminus
991 (blue) to C-terminus (red) according to Figure 2.
992
993 **Supplementary Figure 11 Expression of Zt-KP4-1, Zt-KP4-2, Zt-KP4-3, Zt-KP6-1,**
994 **Zt-KP6-2, Zt-KP6-4 and Zt-KP6-6 during infection of wheat leaves infection.**
995 RNAseq data from Rudd et al. (2015). RPKM (fungal RNAseq Reads Per Kilobase
996 Million)
997
998

999 **Supplementary Table 1. X-ray data collection and refinement statistics for Zt-**
1000 **KP6-1 and Zt-KP4-1**
1001
1002 **Supplementary Table 2. NMR and refinement statistics for Zt-KP6-1**
1003 (Zt-KP6-1, 0.7 mM, 20 mM NaCitrate pH 5.4, 150 mM NaCl, 1 mM DTT, 303 K, 800
1004 MHz) PDB:9GWD BMRB ID 34963
1005
1006
1007 **Supplementary Table 3 List of the proteins structurally related to Zt-KP6-1**
1008 **detected using our pipeline**
1009
1010 **Supplementary Table 4 List of the proteins structurally related to Zt-KP4-1**
1011 **detected using our pipeline**
1012
1013 **Supplementary Table 5 Prediction of the antimicrobial activity of fungal KP4 and**
1014 **KP6 proteins using AMAPEC [88] .**
1015
1016 **Supplementary file S1 Nucleotide sequence of synthetic genes and plasmids**
1017 **used in this study**
1018

1019 **References**

1020 1. Lo Presti L, Lanver D, Schweizer G, Tanaka S, Liang L, Tollot M, et al. Fungal
1021 effectors and plant susceptibility. Annu Rev Plant Biol. 2015;66: 513–545.
1022 doi:10.1146/annurev-arplant-043014-114623
1023 2. Li G, Newman M, Yu H, Rashidzade M, Martínez-Soto D, Caicedo A, et al. Fungal
1024 effectors: past, present, and future. Curr Opin Microbiol. 2024;81: 102526.
1025 doi:10.1016/j.mib.2024.102526
1026 3. Outram MA, Figueroa M, Sperschneider J, Williams SJ, Dodds PN. Seeing is
1027 believing: Exploiting advances in structural biology to understand and engineer plant
1028 immunity. Curr Opin Plant Biol. 2022;67: 8. doi:10.1016/j.pbi.2022.102210
1029 4. Lazar N, Mesarich CH, Petit-Houdenot Y, Talbi N, Li De La Sierra-Gallay I, Zélie E,
1030 et al. A new family of structurally conserved fungal effectors displays epistatic interactions
1031 with plant resistance proteins. Kobe B, editor. PLOS Pathog. 2022;18: e1010664.
1032 doi:10.1371/journal.ppat.1010664
1033 5. de Guillen K, Ortiz-Vallejo D, Gracy J, Fournier E, Kroj T, Padilla A. Structure
1034 Analysis Uncovers a Highly Diverse but Structurally Conserved Effector Family in
1035 Phytopathogenic Fungi. PLOS Pathog. 2015;11: e1005228. doi:10.1371/journal.ppat.1005228
1036 6. Le Naour—Vernet M, Charriat F, Gracy J, Cros-Arteil S, Ravel S, Veillet F, et al.
1037 Adaptive evolution in virulence effectors of the rice blast fungus *Pyricularia oryzae*. PLOS
1038 Pathog. 2023;19: e1011294. doi:10.1371/journal.ppat.1011294
1039 7. Lahfa M, Barthe P, De Guillen K, Cesari S, Raji M, Kroj T, et al. The structural
1040 landscape and diversity of *Pyricularia oryzae* MAX effectors revisited. PLOS Pathog.
1041 2024;20: e1012176. doi:10.1371/journal.ppat.1012176
1042 8. Spanu PD. Cereal immunity against powdery mildews targets RNase-Like Proteins
1043 associated with Haustoria (RALPH) effectors evolved from a common ancestral gene. New
1044 Phytol. 2017;213: 969–971. doi:10.1111/nph.14386
1045 9. Pennington HG, Jones R, Kwon S, Bonciani G, Thieron H, Chandler T, et al. The
1046 fungal ribonuclease-like effector protein CSEP0064/BEC1054 represses plant immunity and
1047 interferes with degradation of host ribosomal RNA. PLOS Pathog. 2019;15: e1007620.
1048 doi:10.1371/journal.ppat.1007620
1049 10. Bauer S, Yu D, Lawson AW, Saur IML, Frantzeskakis L, Kracher B, et al. The
1050 leucine-rich repeats in allelic barley MLA immune receptors define specificity towards
1051 sequence-unrelated powdery mildew avirulence effectors with a predicted common RNase-
1052 like fold. Kobe B, editor. PLOS Pathog. 2021;17: e1009223.
1053 doi:10.1371/journal.ppat.1009223
1054 11. Cao Y, Kümmel F, Logemann E, Gebauer JM, Lawson AW, Yu D, et al. Structural
1055 polymorphisms within a common powdery mildew effector scaffold as a driver of coevolution
1056 with cereal immune receptors. Proc Natl Acad Sci U S A. 2023;120: e2307604120.
1057 doi:10.1073/pnas.2307604120
1058 12. Blondeau K, Blaise F, Graille M, Kale SD, Linglin J, Ollivier B, et al. Crystal
1059 structure of the effector A vr L m4–7 of *Leptosphaeria maculans* reveals insights into its
1060 translocation into plant cells and recognition by resistance proteins. Plant J. 2015;83: 610–
1061 624. doi:10.1111/tpj.12913
1062 13. Lazar N, Mesarich CH, Petit-Houdenot Y, Talbi N, de la Sierra-Gallay IL, Zélie E, et
1063 al. A new family of structurally conserved fungal effectors displays epistatic interactions with
1064 plant resistance proteins. Plant Biology; 2020 Dec. doi:10.1101/2020.12.17.423041
1065 14. Talbi N, Fokkens L, Audran C, Petit-Houdenot Y, Pouzet C, Blaise F, et al. The
1066 neighbouring genes *AvrLm10A* and *AvrLm10B* are part of a large multigene family of
1067 cooperating effector genes conserved in *Dothideomycetes*and *Sordariomycetes*. Mol Plant
1068 Pathol. 2023;24: 914–931. doi:10.1111/mpp.13338

1069 15. Loubet C, Li de la Sierra-Gallay I, van Tilbeurgh H, Fudal I. Decoding plant pathogen
1070 strategies: exploring *Leptosphaeria maculans* effector structural insights for enhanced plant
1071 resistance. Forthcoming. 2024.
1072 16. Yu DS, Outram MA, Smith A, McCombe CL, Khambalkar PB, Rima SA, et al. The
1073 structural repertoire of *Fusarium oxysporum f. sp. lycopersici* effectors revealed by
1074 experimental and computational studies. elife; 2023 Jul. doi:10.7554/eLife.89280.1
1075 17. Teulet A, Quan C, Evangelisti E, Wanke A, Yang W, Schornack S. A pathogen
1076 effector FOLD diversified in symbiotic fungi. New Phytol. 2023;293: 1127–1139.
1077 doi:10.1111/nph.18996
1078 18. Rocafort M, Bowen JK, Hassing B, Cox MP, McGreal B, de la Rosa S, et al. The
1079 *Venturia inaequalis* effector repertoire is dominated by expanded families with predicted
1080 structural similarity, but unrelated sequence, to avirulence proteins from other plant-
1081 pathogenic fungi. BMC Biol. 2022;20: 246. doi:10.1186/s12915-022-01442-9
1082 19. Jumper J, Evans R, Pritzel A, Green T, Figurnov M, Ronneberger O, et al. Highly
1083 accurate protein structure prediction with AlphaFold. Nature. 2021;596: 583–589.
1084 doi:10.1038/s41586-021-03819-2
1085 20. Seong K, Krasileva KV. Prediction of effector protein structures from fungal
1086 phytopathogens enables evolutionary analyses. Nat Microbiol. 2023;8: 174–187.
1087 doi:10.1038/s41564-022-01287-6
1088 21. Derbyshire MC, Raffaele S. Surface frustration re-patterning underlies the structural
1089 landscape and evolvability of fungal orphan candidate effectors. Nat Commun. 2023;14:
1090 5244. doi:10.1038/s41467-023-40949-9
1091 22. Rudd JJ, Kanyuka K, Hassani-Pak K, Derbyshire M, Andongabo A, Devonshire J, et
1092 al. Transcriptome and metabolite profiling of the infection cycle of *Zymoseptoria tritici* on
1093 wheat reveals a biphasic interaction with plant immunity involving differential pathogen
1094 chromosomal contributions and a variation on the hemibiotrophic lifestyle definition. Plant
1095 Physiol. 2015;167: 1158–1185. doi:10.1104/pp.114.255927
1096 23. Kilaru S, Fantozzi E, Cannon S, Schuster M, Chaloner TM, Guiu-Aragones C, et al.
1097 *Zymoseptoria tritici* white-collar complex integrates light, temperature and plant cues to
1098 initiate dimorphism and pathogenesis. Nat Commun. 2022;13: 5625. doi:10.1038/s41467-
1099 022-33183-2
1100 24. Ben M'Barek S, Cordewener JHG, Tabib Ghaffary SM, van der Lee TAJ, Liu Z,
1101 Mirzadi Gohari A, et al. FPLC and liquid-chromatography mass spectrometry identify
1102 candidate necrosis-inducing proteins from culture filtrates of the fungal wheat pathogen
1103 *Zymoseptoria tritici*. Fungal Genet Biol. 2015;79: 54–62. doi:10.1016/j.fgb.2015.03.015
1104 25. Finkler A, Peery T, Tao J, Bruenn J, Koltin Y. Immunity and resistance to the KP6
1105 toxin of *Ustilago maydis*. Mol Gen Genet. 1992;233: 395–403. doi:10.1007/BF00265436
1106 26. Allen A, Islamovic E, Kaur J, Gold S, Shah D, Smith TJ. The virally encoded killer
1107 proteins from *Ustilago maydis*. Fungal Biol Rev. 2013;26: 166–173.
1108 doi:10.1016/j.fbr.2012.10.001
1109 27. Lapalu N, Lamothe L, Petit Y, Genissel A, Delude C, Feurtey A, et al. Improved gene
1110 annotation of the fungal wheat pathogen *Zymoseptoria tritici* based on combined Iso-Seq and
1111 RNA-Seq evidence. 2023. doi:10.1101/2023.04.26.537486
1112 28. Holm L. DALI and the persistence of protein shape. Protein Sci. 2020;29: 128–140.
1113 doi:10.1002/pro.3749
1114 29. Li N, Erman M, Pangborn W, Duax WL, Park C-M, Bruenn J, et al. Structure of
1115 *Ustilago maydis* Killer Toxin KP6 α-Subunit. J Biol Chem. 1999;274: 20425–20431.
1116 doi:10.1074/jbc.274.29.20425
1117 30. Allen A, Chatt E, Smith TJ. The atomic structure of the virally encoded antifungal
1118 protein, KP6. J Mol Biol. 2013;425: 609–621. doi:10.1016/j.jmb.2012.11.033

1119 31. Koltin Y. The killer system of *Ustilago maydis*: secreted polypeptides encoded by
1120 viruses. Viruses Fungi Simple Eukaryotes. 1988; 209–242.
1121 32. Gu F, Khimani A, Rane SG, Flurkey WH, Bozarth RF, Smith TJ. Structure and
1122 function of a virally encoded fungal toxin from *Ustilago maydis*: a fungal and mammalian
1123 Ca2+ channel inhibitor. Structure. 1995;3: 805–814. doi:10.1016/S0969-2126(01)00215-5
1124 33. Tan K-C, Ferguson-Hunt M, Rybak K, Waters ODC, Stanley WA, Bond CS, et al.
1125 Quantitative variation in effector activity of ToxA isoforms from *Stagonospora nodorum* and
1126 *Pyrenophora tritici-repentis*. Mol Plant-Microbe Interactions®. 2012;25: 515–522.
1127 doi:10.1094/MPMI-10-11-0273
1128 34. Kettles GJ, Bayon C, Sparks CA, Canning G, Kanyuka K, Rudd JJ. Characterization
1129 of an antimicrobial and phytotoxic ribonuclease secreted by the fungal wheat pathogen
1130 *Zymoseptoria tritici*. New Phytol. 2018;217: 320–331. doi:10.1111/nph.14786
1131 35. Lima AM, Azevedo MIG, Sousa LM, Oliveira NS, Andrade CR, Freitas CDT, et al.
1132 Plant antimicrobial peptides: An overview about classification, toxicity and clinical
1133 applications. Int J Biol Macromol. 2022;214: 10–21. doi:10.1016/j.ijbiomac.2022.06.043
1134 36. Badet T, Oggenfuss U, Abraham L, McDonald BA, Croll D. A 19-isolate reference-
1135 quality global pangenome for the fungal wheat pathogen *Zymoseptoria tritici*. BMC Biol.
1136 2020;18: 12. doi:10.1186/s12915-020-0744-3
1137 37. Lemoine F, Correia D, Lefort V, Doppelt-Azeroual O, Mareuil F, Cohen-Boulakia S,
1138 et al. NGPhylogeny.fr: new generation phylogenetic services for non-specialists. Nucleic
1139 Acids Res. 2019;47: W260–W265. doi:10.1093/nar/gkz303
1140 38. Van den Ackerveken GF, Van Kan JA, Joosten MH, Muisers JM, Verbakel HM, De
1141 Wit PJ. Characterization of two putative pathogenicity genes of the fungal tomato pathogen
1142 *Cladosporium fulvum*. Mol Plant Microbe Interact. 1993;6: 210–215. doi:10.1094/mpmi-6-
1143 210
1144 39. Stergiopoulos I, Kourmpetis YAI, Slot JC, Bakker FT, De Wit PJGM, Rokas A. In
1145 Silico Characterization and Molecular Evolutionary Analysis of a Novel Superfamily of
1146 Fungal Effector Proteins. Mol Biol Evol. 2012;29: 3371–3384. doi:10.1093/molbev/mss143
1147 40. Battache M, Lebrun M-H, Sakai K, Soudière O, Cambon F, Langin T, et al. Blocked at
1148 the Stomatal Gate, a Key Step of Wheat Stb16q-Mediated Resistance to *Zymoseptoria tritici*.
1149 Front Plant Sci. 2022;13: 921074. doi:10.3389/fpls.2022.921074
1150 41. Zhang Y, Skolnick J. TM-align: a protein structure alignment algorithm based on the
1151 TM-score. Nucleic Acids Res. 2005;33: 2302–2309. doi:10.1093/nar/gki524
1152 42. Mesarich CH, Ökmen B, Rovenich H, Griffiths SA, Wang C, Karimi Jashni M, et al.
1153 Specific Hypersensitive Response–Associated Recognition of New Apoplastic Effectors from
1154 *Cladosporium fulvum* in Wild Tomato. Mol Plant Microbe Interact. 2018;31: 145–162.
1155 doi:10.1094/MPMI-05-17-0114-FI
1156 43. Khang CH, Berruyer R, Giraldo MC, Kankanala P, Park S-Y, Czymmek K, et al.
1157 Translocation of *Magnaporthe oryzae* effectors into rice cells and their subsequent cell-to-cell
1158 movement. Plant Cell. 2010;22: 1388–1403. doi:10.1105/tpc.109.069666
1159 44. Ebert MK, Rangel LI, Spanner RE, Taliadoros D, Wang X, Friesen TL, et al.
1160 Identification and characterization of *Cercospora beticola* necrosis-inducing effector
1161 CbNip1. Mol Plant Pathol. 2021;22: 301–316. doi:10.1111/mpp.13026
1162 45. Brown DW. The KP4 killer protein gene family. Curr Genet. 2011;57: 51–62.
1163 doi:10.1007/s00294-010-0326-y
1164 46. Lu S, Faris JD. *Fusarium graminearum* KP4-like proteins possess root growth-
1165 inhibiting activity against wheat and potentially contribute to fungal virulence in seedling rot.
1166 Fungal Genet Biol. 2019;123: 1–13. doi:10.1016/j.fgb.2018.11.002
1167 47. Tao J, Ginsberg I, Banerjee N, Held W, Koltin Y, BRUENNl JA. *Ustilago maydis*
1168 KP6 Killer Toxin: Structure, Expression in *Saccharomyces cerevisiae*, and Relationship to

Other Cellular Toxins. Mol Cell Biol. 1990;10: 9.
48. Gage MJ, Bruenn J, Fischer M, Sanders D, Smith TJ. KP4 fungal toxin inhibits growth in *Ustilago maydis* by blocking calcium uptake: KP4 fungal toxin mechanism. Mol Microbiol. 2001;41: 775–785. doi:10.1046/j.1365-2958.2001.02554.x
49. Gage MJ, Rane SG, Hockerman GH, Smith TJ. The virally encoded fungal toxin KP4 specifically blocks L-type voltage-gated calcium channels. Mol Pharmacol. 2002;61: 936–944. doi:10.1124/mol.61.4.936
50. Allen A, Snyder AK, Preuss M, Nielsen EE, Shah DM, Smith TJ. Plant defensins and virally encoded fungal toxin KP4 inhibit plant root growth. Planta. 2008;227: 331–339. doi:10.1007/s00425-007-0620-1
51. Guan Y, Ma L, Wang Q, Zhao J, Wang S, Wu J, et al. Horizontally acquired fungal killer protein genes affect cell development in mosses. Plant J. 2023;113: 665–676. doi:10.1111/tpj.16060
52. Schlaich T, Urbaniak BM, Malgras N, Ehler E, Birrer C, Meier L, et al. Increased field resistance to *Tilletia caries* provided by a specific antifungal virus gene in genetically engineered wheat. Plant Biotechnol J. 2006;4: 63–75. doi:10.1111/j.1467-7652.2005.00158.x
53. Quijano CD, Wichmann F, Schlaich T, Fammartino A, Huckauf J, Schmidt K, et al. KP4 to control *Ustilago tritici* in wheat: Enhanced greenhouse resistance to loose smut and changes in transcript abundance of pathogen related genes in infected KP4 plants. Biotechnol Rep. 2016;11: 90–98. doi:10.1016/j.btre.2016.08.002
54. Deb D, Shrestha A, Maiti IB, Dey N. Recombinant promoter (MUASCsV8CP) driven totiviral killer protein 4 (KP4) imparts resistance against fungal pathogens in transgenic tobacco. Front Plant Sci. 2018;9: 278. doi:10.3389/fpls.2018.00278
55. Clausen M, Kräuter R, Schachermayr G, Potrykus I, Sautter C. Antifungal activity of a virally encoded gene in transgenic wheat. Nat Biotechnol. 2000;18: 446–449. doi:10.1038/74521
56. Park C-M, Bruenn JA, Ganesa C, Flurkey WF, Bozarth RF, Koltin Y. Structure and heterologous expression of the *Ustilago maydis* viral toxin KP4. Mol Microbiol. 1994;11: 155–164. doi:10.1111/j.1365-2958.1994.tb00297.x
57. Santos A, Navascués E, Bravo E, Marquina D. *Ustilago maydis* killer toxin as a new tool for the biocontrol of the wine spoilage yeast *Brettanomyces bruxellensis*. Int J Food Microbiol. 2011;145: 147–154. doi:10.1016/j.ijfoodmicro.2010.12.005
58. Snelders NC, Rovenich H, Thomma BPHJ. Microbiota manipulation through the secretion of effector proteins is fundamental to the wealth of lifestyles in the fungal kingdom. FEMS Microbiol Rev. 2022;46. doi:10.1093/femsre/fuac022
59. Snelders NC, Rovenich H, Petti GC, Rocafort M, van den Berg GCM, Vorholt JA, et al. Microbiome manipulation by a soil-borne fungal plant pathogen using effector proteins. Nat Plants. 2020;6: 1365–1374. doi:10.1038/s41477-020-00799-5
60. Snelders NC, Petti GC, van den Berg GCM, Seidl MF, Thomma BPHJ. An ancient antimicrobial protein co-opted by a fungal plant pathogen for in planta mycobiome manipulation. Proc Natl Acad Sci U S A. 2021;118. doi:10.1073/pnas.2110968118
61. Snelders NC, Boshoven JC, Song Y, Schmitz N, Fiorin GL, Rovenich H, et al. A highly polymorphic effector protein promotes fungal virulence through suppression of plant-associated Actinobacteria. New Phytol. 2023;237: 944–958. doi:10.1111/nph.18576
62. de Jonge R, van Esse HP, Maruthachalam K, Bolton MD, Santhanam P, Saber MK, et al. Tomato immune receptor Ve1 recognizes effector of multiple fungal pathogens uncovered by genome and RNA sequencing. Proc Natl Acad Sci U S A. 2012;109: 5110–5115. doi:10.1073/pnas.1119623109
63. Mesny F, Thomma BP. AMAPEC: accurate antimicrobial activity prediction for fungal effector proteins. bioRxiv. 2024; 2024.01.04.574150. doi:10.1101/2024.01.04.574150

64. Ma L, Houterman PM, Gawehns F, Cao L, Sillo F, Richter H, et al. The AVR2–SIX5 gene pair is required to activate I-2-mediated immunity in tomato. New Phytol. 2015;208: 507–518. doi:10.1111/nph.13455
65. Petit-Houdenot Y, Degrave A, Meyer M, Blaise F, Ollivier B, Marais C-L, et al. A two genes – for – one gene interaction between *Leptosphaeria maculans* and *Brassica napus*. New Phytol. 2019;223: 397–411. doi:10.1111/nph.15762
66. Güntert P. Automated NMR structure calculation with CYANA. Methods Mol Biol Clifton NJ. 2004;278: 353–378. doi:10.1385/1-59259-809-9:353
67. Laskowski RA, MacArthur MW, Moss DS, Thornton JM. PROCHECK: a program to check the stereochemical quality of protein structures. J Appl Crystallogr. 1993;26: 283–291. doi:10.1107/S0021889892009944
68. Bowler MW, Nurizzo D, Barrett R, Beteva A, Bodin M, Caserotto H, et al. MASSIF-1: a beamline dedicated to the fully automatic characterization and data collection from crystals of biological macromolecules. J Synchrotron Radiat. 2015;22: 1540–1547. doi:10.1107/S1600577515016604
69. Svensson O, Malbet-Monaco S, Popov A, Nurizzo D, Bowler MW. Fully automatic characterization and data collection from crystals of biological macromolecules. Acta Crystallogr D Biol Crystallogr. 2015;71: 1757–1767. doi:10.1107/S1399004715011918
70. Svensson O, Gilski M, Nurizzo D, Bowler MW. Multi-position data collection and dynamic beam sizing: recent improvements to the automatic data-collection algorithms on MASSIF-1. Acta Crystallogr Sect Struct Biol. 2018;74: 433–440. doi:10.1107/S2059798318003728
71. Bowler MW, Svensson O, Nurizzo D. Fully automatic macromolecular crystallography: the impact of MASSIF-1 on the optimum acquisition and quality of data. Crystallogr Rev. 2016;22: 233–249. doi:10.1080/0889311X.2016.1155050
72. Nurizzo D, Bowler MW, Caserotto H, Dobias F, Giraud T, Surr J, et al. RoboDiff: combining a sample changer and goniometer for highly automated macromolecular crystallography experiments. Acta Crystallogr Sect Struct Biol. 2016;72: 966–975. doi:10.1107/S205979831601158X
73. Kabsch W. Integration, scaling, space-group assignment and post-refinement. Acta Crystallogr D Biol Crystallogr. 2010;66: 133–144. doi:10.1107/S0907444909047374
74. Evans PR. An introduction to data reduction: space-group determination, scaling and intensity statistics. Acta Crystallogr D Biol Crystallogr. 2011;67: 282–292. doi:10.1107/S090744491003982X
75. Potterton E, Briggs P, Turkenburg M, Dodson E. A graphical user interface to the CCP4 program suite. Acta Crystallogr D Biol Crystallogr. 2003;59: 1131–1137. doi:10.1107/s0907444903008126
76. Winn MD, Ballard CC, Cowtan KD, Dodson EJ, Emsley P, Evans PR, et al. Overview of the *CCP* 4 suite and current developments. Acta Crystallogr D Biol Crystallogr. 2011;67: 235–242. doi:10.1107/S0907444910045749
77. Mueller-Dieckmann C, Bowler MW, Carpentier P, Flot D, McCarthy AA, Nanao MH, et al. The status of the macromolecular crystallography beamlines at the European Synchrotron Radiation Facility. Eur Phys J Plus. 2015;130: 70. doi:10.1140/epjp/i2015-15070-0
78. McCarthy AA, Barrett R, Beteva A, Caserotto H, Dobias F, Felisaz F, et al. ID30B – a versatile beamline for macromolecular crystallography experiments at the ESRF. J Synchrotron Radiat. 2018;25: 1249–1260. doi:10.1107/S1600577518007166
79. Krug M, Weiss MS, Heinemann U, Mueller U. *XDSAPP* : a graphical user interface for the convenient processing of diffraction data using *XDS*. J Appl Crystallogr. 2012;45: 568–572. doi:10.1107/S0021889812011715

80. Sparta KM, Krug M, Heinemann U, Mueller U, Weiss MS. *XDSAPP2.0*. J Appl Crystallogr. 2016;49: 1085–1092. doi:10.1107/S1600576716004416
81. Sheldrick GM. Experimental phasing with *SHELXC* / *D* / *E* : combining chain tracing with density modification. Acta Crystallogr D Biol Crystallogr. 2010;66: 479–485. doi:10.1107/S0907444909038360
82. Pape T, Schneider TR. ıt HKL2MAP: a graphical user interface for macromolecular phasing with ıt SHELX programs. J Appl Crystallogr. 2004;37: 843–844. doi:10.1107/S0021889804018047
83. Vagin A, Teplyakov A. *MOLREP* : an Automated Program for Molecular Replacement. J Appl Crystallogr. 1997;30: 1022–1025. doi:10.1107/S0021889897006766
84. Langer G, Cohen SX, Lamzin VS, Perrakis A. Automated macromolecular model building for X-ray crystallography using ARP/wARP version 7. Nat Protoc. 2008;3: 1171–1179. doi:10.1038/nprot.2008.91
85. Emsley P, Lohkamp B, Scott WG, Cowtan K. Features and development of *Coot*. Acta Crystallogr D Biol Crystallogr. 2010;66: 486–501. doi:10.1107/S0907444910007493
86. Adams PD, Afonine PV, Bunkóczi G, Chen VB, Davis IW, Echols N, et al. PHENIX: a comprehensive Python-based system for macromolecular structure solution. Acta Crystallogr D Biol Crystallogr. 2010;66: 213–221. doi:10.1107/S0907444909052925
87. Afonine PV, Grosse-Kunstleve RW, Echols N, Headd JJ, Moriarty NW, Mustyakimov M, et al. Towards automated crystallographic structure refinement with *phenix.refine*. Acta Crystallogr D Biol Crystallogr. 2012;68: 352–367. doi:10.1107/S0907444912001308
88. Mesny F, Thomma BP. AMAPEC: accurate antimicrobial activity prediction for fungal effector proteins. Microbiology; 2024 Jan. doi:10.1101/2024.01.04.574150